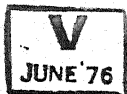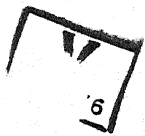# LOW TEMPERATURE SPECIFIC HEAT OF Cr-Fe-Si ALLOYS

A Thesis Submitted
In Partial Fulfilment of the Requirements
for the Degree of
DOCTOR OF PHILOSOPHY
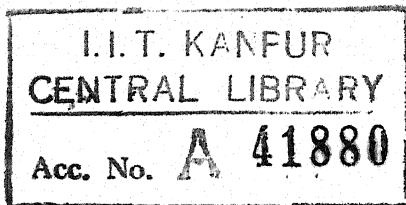
By
SUSANTA KUMAR SI

to the

## DEPARTMENT OF METALLURGICAL ENGINEERING
# INDIAN INSTITUTE OF TECHNOLOGY KANPUR
### SEPTEMBER 1973

ME-1973-D-KUM-LOW

# CERTIFICATE

Certified that the work presented in this thesis
has been carried out under my supervision and that the
work has not been submitted elsewhere for a degree.

(K. P. Gupta)
Professor
Department of Metallurgical Engg.,
Indian Institute of Technology, Kanpur
INDIA

August 27, 1973
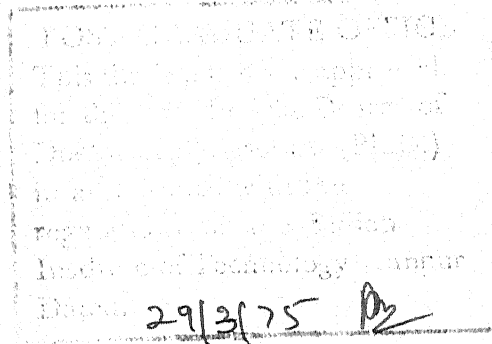
# ACKNOWLEDGEMENTS

The author wishes to express his sincere gratitude to Professor K.P. Gupta for introducing him to the fascinating and challenging field of low temperature research, for his constant guidance and encouragements throughout the work.

Thanks are due to Dr. T.M. Srinivasan who spent innumerable hours with the liquid helium plant for the author, for giving him helps and encouragements in difficult periods; to Dr.R.K.Ray for his valuable suggestions, helps and encouragements.

The author acknowledges with gratitude the fine workmanship of Mr. V.P. Gupta and of Mr. Prithipal Singh in fabricating the apparatus.

It is a pleasure to acknowledge the cooperations received from the staff members of the Low Temperature Laboratory, Mr.S.D. Sarma, Mr. S. Singh, Mr. N. Ahmed; they quickly made him feel a member of the Low Temperature Family.

The author is indebted to Mr. S. Basu for his enthusiasm in preparing the computer programs and data analysis.

The author is thankful to Mr. J.K. Misra for making a neat typescript of the text.

SUSANTA KUMAR SI

CONTENTS

# LIST OF TABLES

# LIST OF FIGURES

## SYNOPSIS

LOW TEMPERATURE SPECIFIC HEAT OF Cr-Fe-Si ALLOYS
A Thesis Submitted
In Partial Fulfilment of the Requirements
For the Ph.D. Degree
by
SUSANTA KUMAR SI
to the
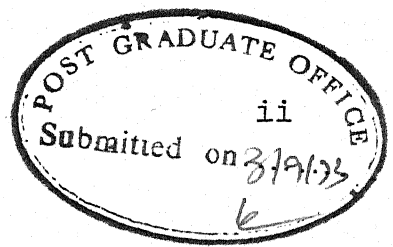Department of Metallurgical Engineering
Indian Institute of Technology, Kanpur
September, 1973

An exchange gas calorimeter, complete with all the accessories for low temperature specific heat measurements in the temperature range of $4.2^{\circ}K$ to about $1.4^{\circ}K$, was set up. To standardise and test the performance of the apparatus, the specific heat of a sample of pure Copper was studied. The electronic specific heat coefficient $\gamma$ and the Debye temperature $\theta_D$ obtained were $1.667 \times 10^{-4}$ cal. mol.$^{-1}$ deg.$^{-2}$ and $341^{\circ}K$, respectively in good agreement with the published results. The accuracy of the calibration of the secondary carbon resistor thermometer was estimated to be better than $\pm 0.001^{\circ}K$. The personal errors were minimised by using the least squares method while the instrumental errors entering the specific heat measurements were estimated to be within $\pm 1\%$ of the measured values.

Low temperature specific heat study of the first long period transition elements indicates that three sub-bands

constitute the d band of these elements. The ternary $(Cr_xFe_{1-x})_{90} Al_{10}$ alloys show that Al present upto about 10 at% have very feeble, if any, interactions with the 3d band of the transition elements. On the other hand experimental results of the low temperature specific heat of the ternary $(Cr_xFe_{1-x})_{80} Al_{20}$ alloys indicate that the apparent effect of increasing Al content to 20 at% is to bring about electron depletion from the 3d band of the transition elements. In this context it was felt that the effect of Si on the 3d band of the b.c.c. transition elements would prove interesting to study.

Low temperature specific heat of a b.c.c. binary alloy $Cr_{97}Si_3$ and a series of nine b.c.c. $(Cr_xFe_{1-x})_{97} Si_3$ alloys covering the entire spectrum from Cr to Fe were investigated. The results for the $Cr_{97}Si_3$ binary alloy indicate that the electronic specific heat coefficient $\gamma$ as well as the lattice specific heat coefficient $\beta$ are increased when Si is dissolved in Cr. Out of the nine ternary alloys, six alloys covering the composition range from $(Cr_{95}Fe_5)_{97} Si_3$ to $(Cr_{70}Fe_{30})_{97} Si_3$ showed anomaly at low temperatures when C/T were plotted against $T^2$. All the alloys except the $(Cr_{90}Fe_{10})_{97}Si_3$ alloy showed upturn anomaly and could be interpreted in terms of super paramagnetic cluster effects. The alloy $(Cr_{90}Fe_{10})_{97} Si_3$, on the contrary, showed downward droop at low temperatures indicating possibly its complex magnetic structure. The remaining three alloys $(Cr_{50}Fe_{50})_{97}Si_3$,

$(Cr_{25}Fe_{75})_{97}$ $Si_3$ and $(Cr_5Fe_{95})_{97}Si_3$ showed normal straight line $C/T$ vs. $T^2$ plots. The electronic specific heat coefficients $\gamma$ for the ternary $(Cr_xFe_{1-x})_{97}$ $Si_3$ alloys were plotted against the transition metal electron concentration $e/a$.

A comparison with the similar plot for the binary $(Cr_xFe_{1-x})$ alloys shows that the curve for the ternary $(Cr_xFe_{1-x})_{97}$ $Si_3$ alloys has shifted towards lower transition element electron concentration. This indicates probable filling up of the 3d band vacancies by the conduction electrons of Si.

# CHAPTER I

## INTRODUCTION

Hume-Rothery's[1,2] realisation of the regularities, in
terms of the valence electron concentration e/a, in the occurrence
of the primary solid solubility limit and the intermediate phases
of alloys based on the noble metals with the polyvalent group B
elements, and Jones'[3] subsequent interpretation of this in terms
of Brillouin-Zone Fermi surface interactions, continue to be
important concepts in the theory of alloy phases. Although the
simple regularities of appearance of phases in the alloys of the
noble metals with the group B elements are not always realised
in the alloys of the other metals, the occurrence and the stabi-
lity of many alloy phases, including those of the transition
elements, are found to exhibit at least a partial dependence
on the electron concentration[4]. While electron concentration has
been realised as one of the factors responsible for the stabi-
lity of a phase, its definition remains rather ambiguous,
especially for the transition metals because of their peculiar
electronic structures. According to Hume-Rothery[2] FeAl, CoAl,
NiAl are 3/2 compounds provided the transition elements are
assumed to have zero valence. On the other hand Raynor[5] observed
in the alloys of Cr, Mn, Fe, Co, Ni with Al that the same phase
appears at the compositions $CrAl_7$, $MnAl_6$, $FeAl_3$, $Co_2Al_9$, $NiAl_3$,
and these compositions correspond to a constant e/a ratio,
except for $FeAl_3$, provided the Pauling's electron vacancy

numbers for the transition elements were used as negative
valence in the e/a calculations; the implications being that
some of the electrons from the Al atoms are transferred to fill
the vacant 3d states of the transition elements. Of the alloys
consisting of the transition elements only, the compositions of
the α-Mn and the σ-phases in various binary systems shift in
such a way as to correspond approximately to a constant elec-
tron concentration. Appearance of the other transition metal
complex phases, like the P, R, μ , β-Mn phases, over narrow
ranges of compositions across the ternary phase diagrams indicates
their sharp dependence on electron concentration[4]. The importance
of electron concentration in the stability of the Laves phases,
a traditional size factor compound, has been recognised[6] and
demonstrated[7,8]. Low temperature specific heat data[9] on the
Laves phases of ternary systems substantiate the earlier conten-
tion[6] that the preference of a particular Laves phase type over
the others depends on electron concentration.

The alloying behaviour of the non-transition elements,
particularly Al and Si, with the transition elements reveals
some important features[4]. A complex phase like the σ -phase,
thought to be formed when both the elements are transition
elements, is found to be formed by several of the transition
elements with Al. An analogous example is the formation of the
R-phase in binary systems with Si as the second element. In
ternary alloys in which a non-transition element is the third
element, many of the complex phase fields are extended considera-
bly. It is also found that the binary systems in which these

phases are expected but donot form, get stabilised by addition of Al and Si. These behaviours could be explained[10] by considering charge contributions from the non-transition elements.

The theoretical interpretations of Jones[3,11], and more recently by Hume-Rothery and Roaf[12], on the correlation between e/a ratio and phase stability are based on the rigid band approximation. Since the rigid-band approximation is based on first order perturbation in which the variation of the band shape with composition is ignored, theoretically such a correlation continues to remain unsatisfactory. Recently Blandin[13,14] and Heine[15] have made, employing second order perturbation for calculating energy, fresh attempts to correlate e/a ratio with the stability of alloy phases. However, the situation appears[16] to be that neither the traditional ideas nor the recent theories give a satisfactory explanation of the stability of alloy phases in terms of electron concentration per atom.

Even in the absence of adequate theoretical justifications till now, the vast experimental data available on alloy phases indicate that the extent of the stability of alloy phases does depend on some kind of charge sharing between the constituent elements. To substantiate such conjectures, based mainly on phase equilibria work, experiments which give direct informations about the electronic structures have to be carried out. Photo emission spectroscopy, soft X-ray spectroscopy, low temperature specific heat, to name a few of the many techniques available now are being widely used for studying the electronic structure of

metals and alloys. In the light of new data being made available
by these experimental techniques, many of the traditional concepts
on the alloy phases are bound to come under fresh assessment and
review. A couple of examples may be quoted as illustrations.
Photo emission study of Ni and Ni-Cu[17-18] alloys indicate that
atleast for the lower range of Ni concentrations the rigid band
model does not appear to hold good in this alloy system. Experi-
mental evidences point rather towards the possibility of localised
states of Ni 3d levels between the Fermi level and the top of
3d band density of states of Cu. Recently soft X-ray spectroscopy
of transition metal-Al alloys has been employed[19] to investigate
the electron transfer from Al atoms to the vacant 3d states of
Mn, Fe, Co and Ni. The data indicate that the 3d band vacant
states in Mn, Fe, Co, Ni are progressively filled by the valence
electrons of Al as its concentration increases. This is in
contrast with what has been observed in the specific heat data
of Fe-Cr-Al alloys.[34,36,37] However, there exists no one to one
correspondence between the number of valence electrons available
from the Al atoms at a certain composition and the number of
vacant 3d states being filled by them.

Low temperature specific heat data, as already mentioned,
is also quite useful in studying the electronic structure of
metals and alloys. It has been widely used for studying the
structure of d band of the transition metals, and their alloys
with the other transition metals[21,22] or with the non-transition
metals[34,36,37]. In the Bethe-Sommerfeld theory of metals, the

electronic specific heat at low temperature is linear in temperature in the first order approximation. The lattice specific heat is proportional to $T^3$ when $T < \theta_D$, where $\theta_D$ is the Debye temperature. Therefore, in the absence of any other contribution, the total specific heat is given as:

$$C = \gamma T + \beta T^3 \tag{1.1}$$

where $\gamma$ and $\beta$ are the electronic and the lattice specific heat coefficients, respectively. In this theory $\gamma$ is proportional to the electronic density of states $N(E_F)$ at the Fermi level and is given by:

$$\gamma = 2/3 \, \pi^2 \, \alpha \, k^2 \, N(E_F) \tag{1.2}$$

where 2 is for both the spin directions, k is the Boltzmann constant, and $\alpha$ is a numerical factor determined by the units used for $\gamma$, $N(E_F)$ and k. Therefore, the value of the electronic specific heat coefficient $\gamma$ is a measure of the density of states at the Fermi level of a metal or an alloy.

The experimental data of the $\gamma$ values of binary alloys of the first long period transition elements have been plotted as a function of their average group numbers[21]. Within the frame work of rigid-band approximation this $\gamma$ vs. e/a plot should represent the density of states of the d band of the first long period transition elements. This $\gamma$ vs. e/a plot shows prominent maxima and minima in the range of e/a from 4 to 9[21]. There is a maximum at e/a = 4.5, followed by two minima, one at e/a = 6 and

the other at e/a = 8.3.  There is a very sharp peak at e/a = 6.4.
The prominent features in the $\gamma$ vs. e/a curve correlate well
with those of the Slater-Pauling curve.[66]  The minimum of the
electronic specific heat coefficient at e/a = 6, coincides with
the first appearance of a spontaneous moment, and the second
minimum at e/a = 8.3 coincides with the maximum value of the
spontaneous moment.  On the basis of the low temperature speci-
fic heat and the magnetic moment data it was concluded[22] that
the region of high electronic specific heat  at e/a < 6 corres-
ponds to a 3d sub-band with paired spin up and spin down electron
states.  The region of high electronic specific heat, at 6<e/a <8.3
may be associated with a second 3d sub-band with one spin direc-
tion only; and the rise of electronic specific heat at e/a > 8.3
may be associated with a third 3d sub-band characterised by a
spin orientation opposite to: that in the second sub-band.

The low temperature specific heat data together with the
magnetic moment data indicate that the rigid-band model is quite
satisfactory for the b.c.c. alloys of the 3d transition elements.[23]
In recent years, however, it has become increasingly · evident[24]
that the many-body effects in particular the electron-phonon
interactions, will increase  the measured electronic specific
heat coefficient over the one electron band-structure value by
an enhancement factor of $(1 + \lambda)$, where $\lambda$ is defined by the
relation:

$$m_b^* = m_b(1 + \lambda) \qquad (1.3)$$

$m_b^*$ is the effective mass when electron-phonon interactions are
added to the one-electron band mass $m_b$. Estimates of the enhance-
ment factor $\lambda$ for several metals undergoing superconducting
transition and the noble metals and their alloys[24-28]
indicate that it is specially important for metals with high
density of states at the Fermi level. However, for most of the
metals and their alloys an estimate of $\lambda$ value is not available.
As a result the band shape derived from the experimentally deter-
mined electronic specific heat data is subject to some uncertainty,
the extent of which is difficult to evaluate at the present time.
This uncertainty, therefore, is expected to contest the expecta-
tion that the prominent features in the experimentally determined
$\gamma$ vs. e/a plot for the 3d transition metals and their alloys
are characteristics of the band structure of the transition metals
concerned. McMillan[29] suggested that the electron-phonon enhance-
ment factor should depend heavily on the phonon frequency spec-
trum of the system concerned. The elastic constants, and
therefore, the phonon frequencies, are not known to undergo
drastic changes with composition in the solid solution alloys
of the neighbouring 3d transition elements. Hence, Beck[24] con-
cluded that the prominent features in the $\gamma$ vs. e/a curve of
these 3d elements and their alloys reflect the corresponding
variations in their density of states, even though the relative
magnitudes of the various maxima and minima may get altered to
some extent by the electron-phonon interactions. On this basis,
therefore, it is reasonable to expect that even in the absence

of the detailed knowledge of many-body effects, one can delineate
a semi-quantitative picture of the structure of the 3d band with
a considerable degree of confidence.

To determine if the non-transition elements contribute
electrons to the 3d band, electronic specific heat of a series
of alloys of 3d elements with non-transition elements were
measured[30]. The results show a sharp decrease in $\gamma$ of V-Al,
V-Sn, V-Sb alloys with increase in the non-transition solute
element concentration, indicating a possible rigid-band behaviour.
However, a series of $(Ti_{0.7} V_{0.3})_x Al_{1-x}$ alloys[30] donot show the
initial anticipated increase in the $\gamma$ values with increase in
Al content of the alloy. If one assumes rigid-band model one
would expect that addition of the non-transition elements Al,
Sn, Si, Sb to Fe should decrease $\gamma$. The specific heat data on
Fe alloys, however, show[31,32] that the $\gamma$ values practically
donot change (actually it increases slightly). These specific
heat data cannot be interpreted as a simple filling of the 3d
band by the non-transition element valence electrons, but they
suggest localisation of the valence electrons at the solute
atom sites; a fact consistent with the magnetic data on these
alloys[33,65]. Thus the low temperature specific heat data on
the V and Fe alloys with the non-transition elements indicate
that the non-transition elements interact with the first 3d
sub-band but not with the second 3d sub-band. A confirmation
of this conclusion also emerges from a series of papers by Beck
and his associates.[34,36,37] Ternary alloys of b.c.c Ti-V,

V-Cr, Cr-Fe, Fe-Co with constant Al additions were studied. When the $\gamma$ values were plotted as a function of the average group number of the transition metal constituents only, the curves show that for the alloys with 10 at% Al, the non-magnetic sub-band is affected, whereas the magnetic second and the third sub-bands remain essentially unchanged.[34] The lowering of $\gamma$ in the first 3d sub-band was explained[34] in terms of a reduction of the number of states in that sub-band in the presence of Al.

The b.c.c. alloys of the transition metals with 20 at% Al, however, produce a different picture. The prominent features in the $\gamma$ vs. e/a plot for the alloys with 20 at% Al are displaced with respect to those of the alloys without Al[21], indicating that the addition of 20 at% Al introduces a change in the 3d band of the transition elements. Since the displacement takes place towards higher transition metal electron concentration, it indicates removal of 3d electrons so that the filling up of the third 3d sub-band starts at a higher transition element electron concentration than in the alloys without Al or with 10 at% Al. The extent of the shift as calculated from the displacement of the maximum at e/a = 8.0 corresponds to a loss of about 0.05 to 0.1 electrons from the 3d band. This is consistent with the magnetic data of the Fe-Al alloys[33], which show that the addition of 20 at% Al leads to a decrease of about $0.07 \mu_B$ per Fe atom. According to the model of ferromagnetism by Gupta et al.[22] this would mean a loss of about 0.07 electrons from the second 3d sub-band of Fe. The lowering of the minimum at e/a = 6 was explained[36,37] to be

the result of the shifting away from each other of the first and the second 3d sub-bands, which slightly overlap at Cr. Lowering of $\gamma$ value in the b.c.c Cr-Al alloys[34] (20 to 25 at% Al) to a value lower than that for pure Cu also corroborates this idea of band shifting. As the Al content is increased to 30 at%, the two sub-bands are shifted back towards each other and the overlap between them is re-established[38]. Transport properties of Cr-Al alloys[38] for 0.2 to 33.3 at% Al content support these interpretations in terms of band shift.

In the same context of charge transfer from the non-transition elements to the vacant 3d states of the first long period transition elements, the transition metal borides present some interesting features. On the basis of their physical properties, including the magnetic properties,[39-42] it has been suggested that the band structure of the transition metal remains approximately the same as boron enters the lattice to form the compound, and that the boron atom donates electrons to the 3d band of the transition metal, thereby raising the Fermi level over its position in the pure metal. However, subsequent low temperature specific heat study of the half, mono and the diborides show that their $\gamma$ vs. e/a plot donot resemble that for the alloys involving the transition elements of the first long period. This refutes the earlier suggestions that the 3d band of the first long period transition elements do not appreciably change when boron atoms enter the lattice to form compounds.

Out of the several polyvalent non-transition elements, the alloying behaviour of Al and Si with the transition elements has been more widely studied. The stabilising effect of these two elements on the complex intermediate phases of the transition elements is generally recognised to be due to some 'electronic factor'. If this conjecture is correct, then the presence of Si should be reflected in the electronic structure of the alloys of the transition metals in which it is present as a solute element. Already some work has been done to determine the effect of Al on the electronic structure of the transition metals and their alloys. The present work on the low temperature specific heat of the b.c.c. Cr-Fe alloys with 3 at% Si was under-taken to study the effect of Si on the electronic structure of the first long period transition metals.

# CHAPTER II

## EXPERIMENTAL APPARATUS

### 2.1 General Criteria for Design:

The specific heat of a substance can be estimated by measuring its temperature increment resulting from the introduction of a known quantity of thermal energy. In this method it is necessary that the specimen is thermally isolated from its surroundings such that there is no heat loss from the specimen to the surroundings. A calorimeter utilising this condition is known as an adiabatic calorimeter.

In specific heat study at low temperature the temperature range of investigation is generally confined to 1.4 $^{\circ}$K to 4.2 $^{\circ}$K. Since the boiling point of liquid He, as that of any other liquid, is fixed by its vapour pressure, it is possible to achieve this temperature range bycontrolling the vapour pressure over the liquid He bath by pumping through a manifold of control valves and a mamostat. After reaching the lowest temperature the thermal isolation of the specimen can be achieved by producing high vacuum (of the order of $10^{-6}$ torr.) inside the calorimeter. The heater and the thermometer both have to be kept in thermal contact with the specimen. The thermal energy to the specimen can be supplied by passing for a definite time interval a constant current through a heater coil. The temperature is quite commonly measured by the secondary thermometers like

carbon or germanium resistors calibrated against the temperature of the liquid He bath at varying vapour pressures. The secondary thermometers are calibrated using the He vapour pressure scale either using the vapour pressure of the He bath or providing a He bulb near the thermometer. The thermometer resistance is measured employing a D.C. potentiometer together with accessories for efficient operations. In most of the laboratories He is used in a close circuit. The evaporated gas is collected in a gas bag through a recovery line connected to the liquid He dewar, purified and stored in cylinders for re-liquifaction.

Based on the requirements mentioned above, the present experimental equipment for low temperature specific heat study constituted a cryostat to attain temperatures in the range of $4.2^{\circ}K$ to about $1.4^{\circ}K$, a calorimeter to provide thermal isolation of the specimen, a heater to supply heat in the form of electrical energy, a thermometer to measure temperature, and the necessary accessories.

## 2.2 Equipment Design and Description:

## 2.2.1 Cryostat:

As shown in Figure 1, the cryostat constituted an assembly of two glass dewars and a metal top. The outer liquid nitrogen dewar ( 7, Figure 1) was of 6" I.D x 8 $\frac{1}{2}$ " O.D. x 28 $\frac{1}{2}$ " over-all height with two vertical slit-windows, about 3/8" wide, running all along the length on two opposite sides of the dewar for observations. The inner liquid He dewar ( 6, Figure 1) was of

$2\frac{1}{4}$ " I.D x $4\frac{1}{2}$ " O.D x 30" over all height. It was fitted with a 3 mm glass stop cock for evacuation of the space enclosed between the double walls. Two vertical slit windows, 3/16" wide, run all along the double walled portion of the dewar. The double walled He dewar ended at its top with a single wall extension. A kovar ring, one end of which was silver soldered to a 1/4" thick x 4 1/2" diameter brass flange with a $2\frac{3}{4}$ " O-ring groove was sealed to this single walled dewar neck.

The cryostat was housed in a table of dimensions 22 "x 12 "x 33 1/2 ", made from 1.5" angle iron. Liquid He dewar was suspended from the table top of 1/4" thick aluminium plate ( 4. Figure 1). To facilitate easy with drawal of the He dewar the aluminium table-top plate was made in two pieces. The He dewar with the metal top of the cryostat was held rigidly on the aluminium plate with six 1/4" brass bolts. The table height was fixed such that in the cryostat assembly the glass stop cock of the He dewar was well above the brim of the liquid nitrogen dewar, and the clearance between the bottom of the two dewars was about 1.0 ". A 3/8 " diameter hole was made in the aluminium plate for insertion of the liquid nitrogen syphon as also for introducing a polythene tube down to the bottom of the liquid nitrogen dewar for drawing out collected water at regular intervals. The draining out of water from liquid nitrogen dewar was a routine job for dewar protection, found specially necessary in humid weather.

TO DIFFUSION PUMP

TO CONTROLLING VALVES

TO MANOMETER

TO PUMP

1. METAL CAP
2. He INTAKE
3. MULTITERMINAL HEADER
4. ALUMINIUM PLATE
5. METAL TO GLASS SEAL
6. LIQ. He DEWAR
7. LIQ. $N_2$ DEWAR
8. THINWALLED STAINLESS STEEL TUBE
9. CARBON RESISTOR
10·HEATER THERMOMETER ASSEMBLY
11 SPECIMEN
12 CALORIMETER
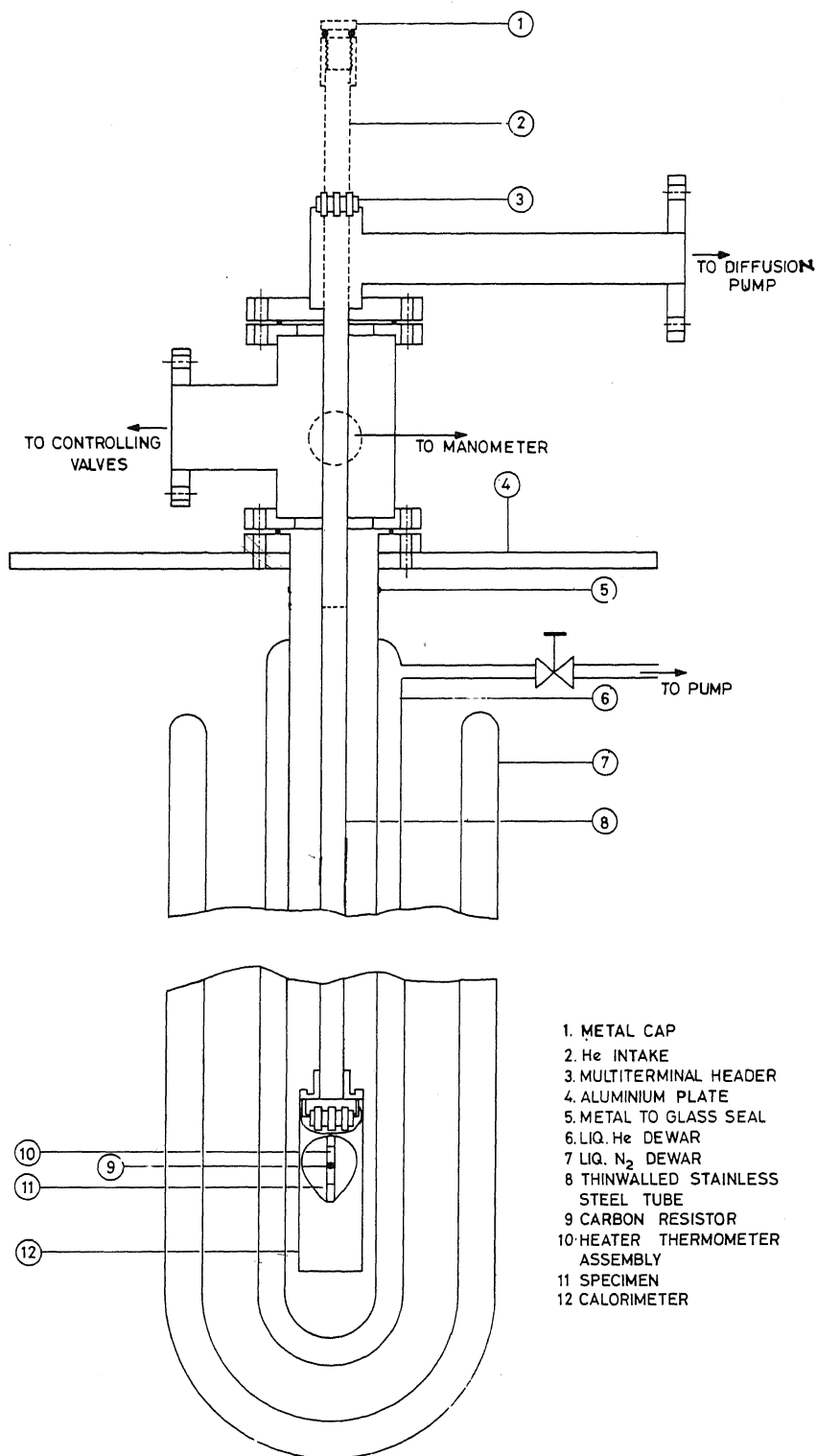
Fig.1 Cryostat for low temperature specific heat measurements

The metal head of the cryostat was rigidly bolted on the He dewar flange forming a leak proof joint. The cryostat head had three outlets, a 2" diameter flanged opening to connect the recovery line as well as the pumping line, a 1" diameter second flanged opening connected to the mercury manometer for registering vapour pressure of the He bath and the third outlet was a small 3/8" diameter copper tube connected with a Hoke needle valve ($V_{11}$, Figure 2). A brass nipple was soldered to the open end of this valve. This outlet was used for several purposes:

(i)     for initial evacuation of the He dewar,

(ii)    to introduce He exchange gas and

(iii)   for connecting the bleeder tube of the liquid He storage dewar before transferring liquid He to the cryostat.

The vacuum jacket and the inside of the He dewar were evacuated by a two stage Duo-Seal mechanical pump (Mech. Pump No. 2 Figure 2) with a pumping capacity of 58 litres/minute and an ultimate vacuum of $2 \times 10^{-2}$ torr. A Veeco thermocouple gauge (T.C.1, Figure 2) was used to monitor the evacuation.

2.2.2 Main Pumping System and the Control Manifold:

(a) Pumping System:

The temperature of the He bath was controlled by pumping over it through a manifold of control valves. A 3" diameter central pumping line (with extensions to all other low temperature apparatus ) was available for pumping above the He bath. This pumping line was connected to a (Model KDH-130) Kinney pump with
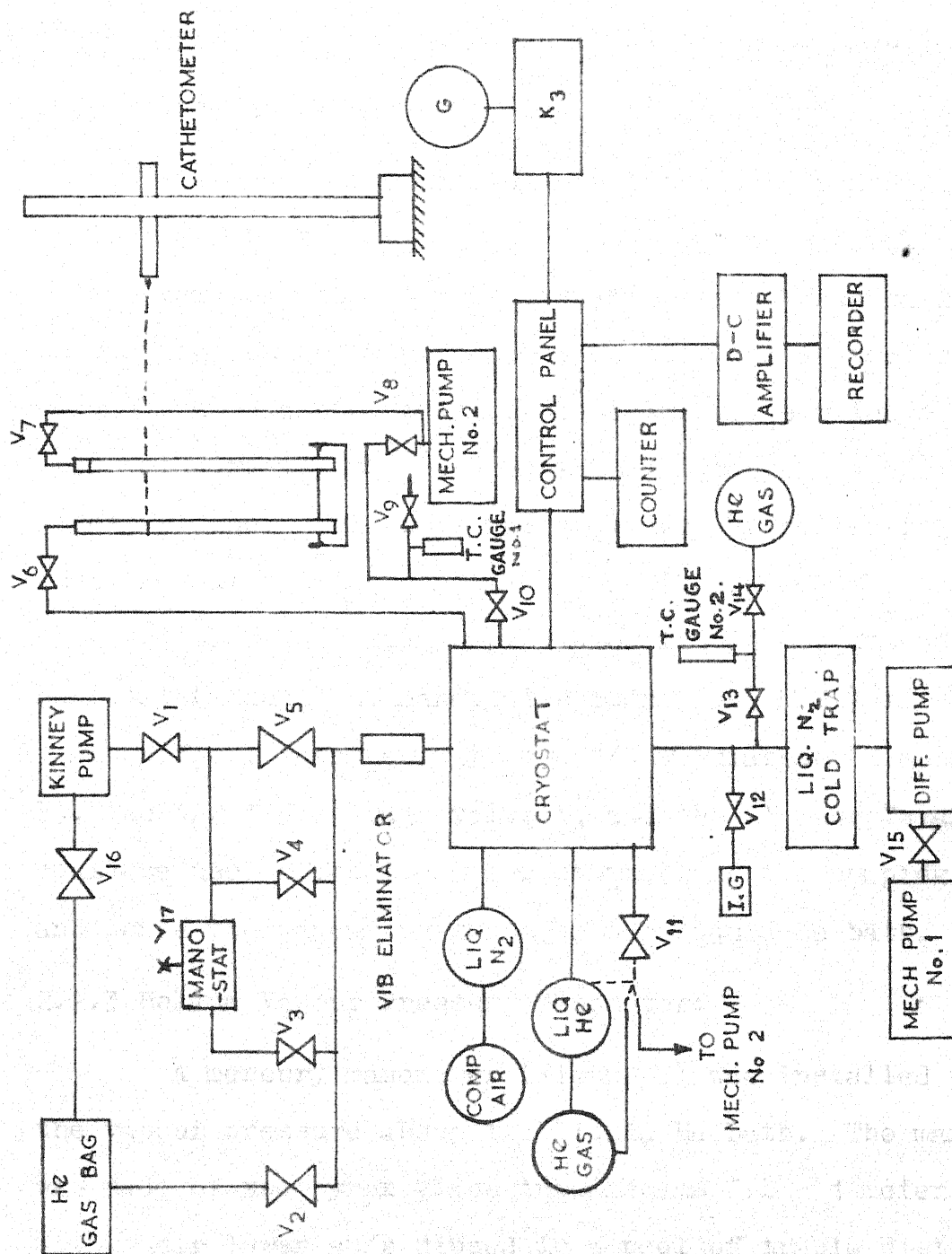
FIG. 2 BLOCK DIAGRAM FOR LOW TEMPERATURE SPECIFIC HEAT MEASUREMENTS.

an ultimate pressure of $10^{-2}$ torr. and a capacity of 130 c.ft/
minute.  The exhaust of the pump was connected through the valve
$V_{16}$ to a gas bag (Figure 2) for collecting the gas for reuse.

(b)  Valve Manifold:

The control manifold, constituting a manostat and a
system of four valves $V_2$, $V_3$, $V_4$, $V_5$ arranged parallel to each
other, was connected to the cryostat head through a 2" diameter
copper pipe and a 2" diameter vibration eliminator. The valve $V_2$
was a 1 1/2" diameter Sylphon diaphragm valve which connected the
cryostat directly to the  He gas bag through a 1 1/2" diameter
recovery line.  This line was provided for collecting He gas
under normal boiling conditions of liquid He.  The valve $V_2$
was kept closed during pumping over liquid He. The cartesian
manostat (model  8, manostat corporation, N.Y.) fitted with a
1 mm orifice, together with the 1/4 "  diameter diaphragm valve
$V_3$, the 1/2 " diaphragm valve $V_4$ and the 2" Cane Y-valve $V_5$
could be used effectively for controlling the pumping speed,
and hence the vapour pressure of the liquid He bath.

2.2.3 Helium Vapour Pressure Manometer:

A mercury manometer (Figure 2) was installed to measure
the vapour pressure above the liquid He bath.  The manometer
was made of two pyrex glass tubes, 14 mm I.D $\times$ 1 meter length,
with their lower ends dipped in a pool of triple distilled
mercury.  The upper end of one tube was connected to the 1" outlet
of the cryostat head through a 3/8 "diameter shut off diaphragm
valve, and the other tube was connected through  a 3/8 "shut off

diaphragm valve to a mechanical pump (Mech Pump No. 2, Figure 2).
The difference in the heights of the mercury columns in the two
tubes indicated the vapour pressure of He.  The heights of the
mercury columns were measured with a cathetometer with a least
count of 0.01 mm, supplied by Gaertner Scientific Corporation,
Chicago, U.S.A.  The cathetometer was placed 9 feet away from the
manometer and levelled properly before taking each reading. Since
the end pressure of the mechanical pump was about $2 \times 10^{-2}$ torr,
which is negligible compared with the accuracy of the cathetometer
it is justifiable to take the difference in the heights of the
two mercury columns as the absolute pressure of He vapour above
the liquid bath.  The elapsed time between taking the two readings
with the cathetometer was typically between 15 to 20 seconds.
Since very slow pumping over liquid He was employed, the change
in the height of the fixed column was found negligible. Hence
the dynamic method of vapour pressure measurement involves no
serious inaccuracy.

## 2.2.4  Calorimeter Assembly:

The calorimeter assembly (Figure 1) consisted of three
major sections: (i) the calorimeter can for accommodating as well
as for thermally isolating the heater-thermometer-specimen
assembly, (ii) a flanged copper tee at the top that could be
coupled to a  vacuum train, and (iii) a 1/2" I.D x 26" long x 0.006
thick stainless steel tubing (  8,Figure 1) connecting the calori-
meter can to the copper tee at the top. The calorimeter can is
evacuated through this tube.

The calorimeter can ( 12, Figure 1) was made of stainless steel tube $1\frac{1}{4}$" O.D. x 4" long x 0.012 "thick, fitted with a 1/32 "thick copper end plate which covered the bottom of the calorimeter can. The open end of the can had a 1/32 " thick machined copper ring such that it fitted snugly on the copper cover plate which was silver soldered to the free end of the 1/2" diameter stainless steel tube. An octal Kovar plug was soft soldered to the calorimeter cover for bringing in the electrical leads to the calorimeter. Since this plug was thermally connected with the He bath, it also functions effectively as a radiation sheld. The calorimeter can was slipped on to the copper cover to facilitate soldering. This was the only joint which had to be opened and resoldered each time a new specimen was put in. Wood's metal was used for making this joint. It had the advantage of having a very low melting point so that the insulation of the lead wires and the tin-lead solder of the neighbouring joints remained unaffected during soldering of the can.

(a) Lead Wire Connections:

During Specific heat measurements it is necessary to thermally isolate the specimen. Therefore, for minimizing heat leak through the lead wires 40 gauge nylon covered Manganin wires were used. Since soldering of these thin wires were difficult and there were chances of their opening up or tearing from the octal Kovar plug, the insulation stripped ends of the Manganin wires were wrapped round a 1" piece of 30 gauge copper wire and soldered to it. The lead wires were ensheathed in thin

teflon spaghetti which snugly fitted to the end copper wires.
The lead wires were passed through the 1/2" diameter stainless
steel tube of the calorimeter assembly and soldered to the
Kovar plug leads. Since single pieces of Manganin wires were
used as lead wires no spurious thermal emf was detected. This
arrangement was found better than using half lengths of 30 gauge
copper wires and Manganin wires for making up the lead wires.
Copper lead wires were soldered to the outer Kovar plug to
connect the calorimeter leads with the instrument panel.

(b)  Heater-Thermometer Assembly:

The heater-thermometer assembly was made for accommodating
the carbon resistor thermometer and the heater coil. The specimen
in two pieces were tied on the two flat sides of this assembly.
These were made from pure copper with a size of 7/16" diameter
and 3/16" thick flats with a 1/2" long extension arm E(Figure 3).
The weight of copper, which was chosen as the structural
material due to its low heat capacity and good thermal conduc-
tivity, was less than 0.06 mole. The carbon resistor thermometer
was chosen for its high negative temperature coefficient at low
temperature and because of its known temperature-resistance
relation.  The thermometer was fitted in the small hole at the
middle of the assembly body (B in Figure 3). The 1/4 watt Allen-
Bradley carbon resistor used as the thermometer had a nominal
room temperature resistance of 56$\Omega$. The external insulation
and the colour coding were removed by wiping with acetone. A
thin coating of clear glyptol lacquer was put on the resistor

before encasing it in the copper block. This coating, on curing for two days, provided a satisfactory electrical insulation and good thermal contact between the carbon thermometer and the copper block. The heater was made with about 10' long 40 gauge nylon insulated Manganin wire. It was wound non-inductively into the peripherial groove of the copper block (C in Figure 3). Four heater and four thermometer leads of nylon covered Manganin wire were provided for connecting the heater thermometer assembly to the octal Kovar plug of the calorimeter.

## (c)  Helium Intake Line:

A helium intake line was provided on the top flange of the calorimeter assembly. Initially this was made of two thin walled stainless steel tubes placed concentrically with a provision for evacuating the space between the two walls. It was provided with a metal cap and an 'O'-ring seal. This intake worked well for first few transfers, but later on developed some microleak undetectable at room temperature and yet sufficient for heat leak at liquid He temperature causing difficulty in liquid He transfer. This double walled intake line was replaced by a single walled 1/2" diameter, 12" long and 0.006" thick stainless steel tube fitted with a metal cap and an 'O'-ring gasket. In this arrangement the delivery end of the transfer syphon itself was pushed through this inlet deep inside the experimental dewar.

Fig. 3   Heater–thermometer–specimen assembly

Ⓐ Copper housing
Ⓑ Thermometer
Ⓒ Heater
Ⓓ Specimen
Ⓔ Extension for heat switch
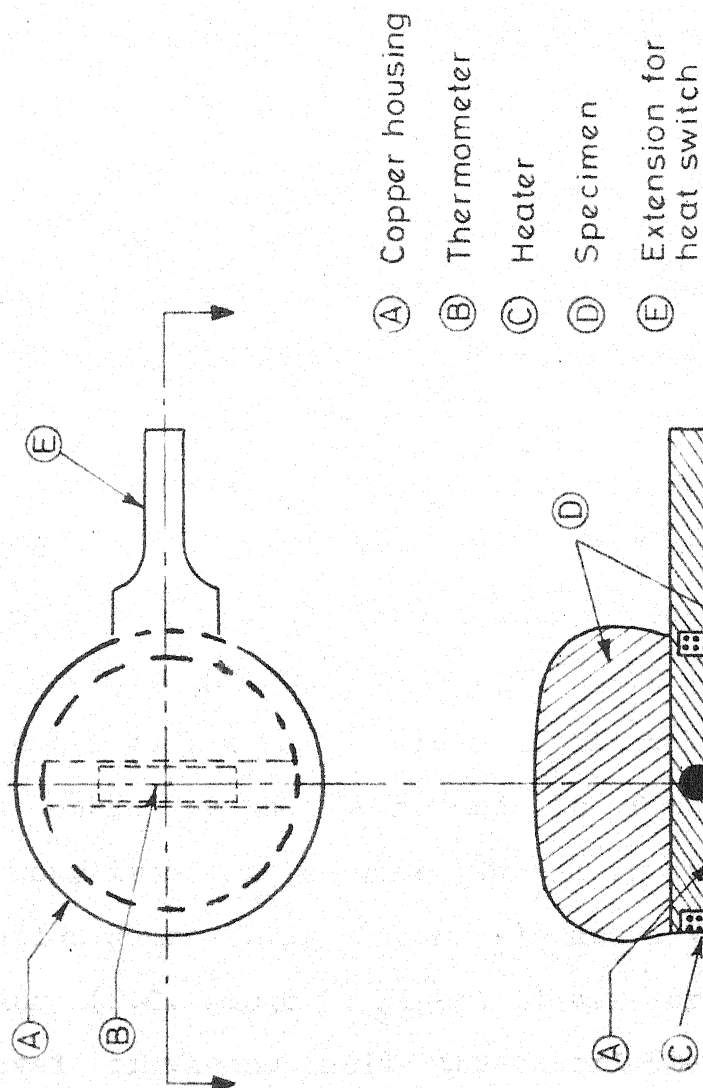
(d) <u>Evacuation Arrangement for the Calorimeter</u>:

In exchange gas calorimeter evacuation prior to putting
He exchange gas inside the calorimeter was necessary. Also a
high vacuum had to be created inside the calorimeter can for
thermalisolation of the specimen.  A vacuum train was assembled
for this purpose (Figure 2).  The vacuum train consisted of
(i) a mechanical pump (Mech. Pump No. 2, Figure 2), (ii) a diffu-
sion pump with accessories, (iii) pressure measuring gauges, and
(iv) an inlet fitted with two valves $V_{13}$, $V_{14}$ (Figure 2) for
putting in the exchange gas. The mechanical pump was a two stage
Due-Seal (Model 1402) pump with a pumping speed of 140 litres /
minute and an ultimate vacuum of $10^{-3}$ torr. The 2" oil diffusion
pump (Veeco, EP-2W ) had a pumping speed of 90 litres/ sec.  and
an ultimate pressure of $2 \times 10^{-9}$ torr. The accessories included
a water cooled baffle and a metallic liquid nitrogen cold trap
for enhancing the vacuum and also for blocking any stray oil
vapour from getting into the calorimeter.  A Veeco  RG-75K ioni-
zation gauge (I.G., Figure 2)  and a Veeco DV-1M  thermocouple
gauge (T.C. gauge 2, Figure 2) were provided to monitor the
level of vacuum inside the calorimeter assembly to which the
vacuum train was connected.  The ionisation gauge and the thermo
couple gauge were fitted with the valves $V_{12}$ and $V_{13}$ (Figure 2)
respectively, to isolate them from the vacuum line.

## 2.2.5 Electrical Circuit:

The principle of measurement of specific heat at low temperature involves a known amount of heat input to the specimen, and the measurement of the corresponding rise in temperature. Heat was supplied in the form of electrical energy $\Delta E = i^2 Rt$, where i was the heating current, R the heater resistance and t the duration of heating current. The temperature was measured by a carbon thermometer calibrated against He vapour pressure above the liquid He bath. Keeping all these requirements in mind the electrical circuit design, adapted from that used by Cheng[45], had the following main features:

(i)     a thermometer circuit for accurate measurement and control of measuring current,

(ii)    a recording branch extending from the thermometer circuit for continuous measurement of e.m.f. across the thermometer,

(iii)   a heater circuit for accurate measurement of heater currents and the heater resistance, and

(iv)    a time measuring device to accurately note the duration of a heat pulse.

### (a) E.M.F. Measurements:

A complete schematic diagram of the electrical circuit and the instruments used is shown in Figure 4. A photograph of the control and the measuring panel is shown in Figure 5. The main measuring instrument was a Leeds and Northrup K-3 potentiometer capable of reading e.m.f. from 0 to 1.6 volts to an accuracy of $\pm (0.015\% + 0.5\mu V)$. A Leeds and Northrup 2430 D
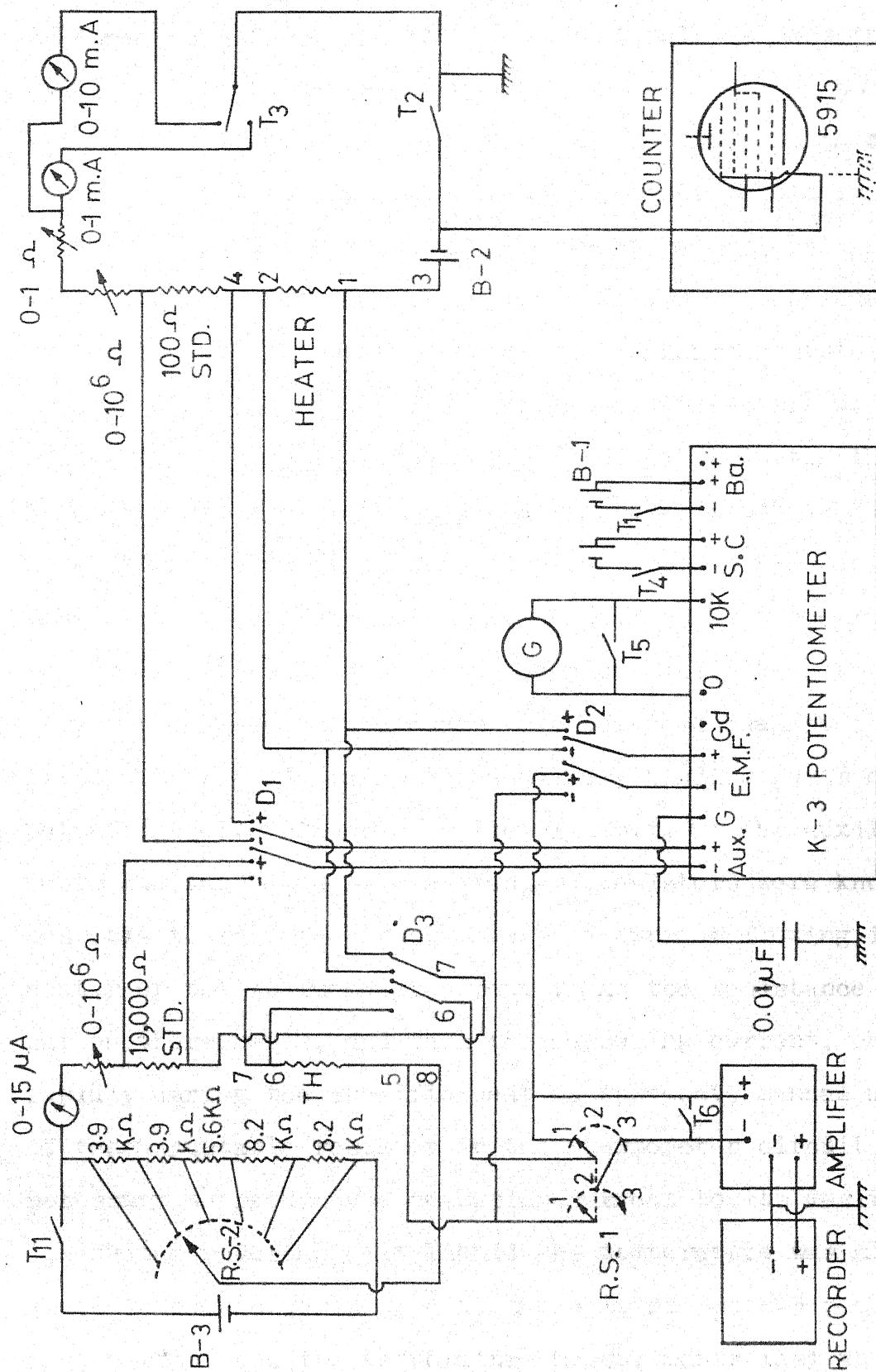
Fig. 4 Wiring diagram for low temperature specific heat measurements

type galvometer (sensitivity 0.0005$\mu$A/mm) was used together
with the potentiometer. Two thermal free D.P.P.T. switches $D_1$,
$D_2$ linked the heater and the thermometer circuits to the poten-
tiometer. A third D.P.D.T. switch $D_3$ was included in the circuit
so that resistivity studies at low temperature could also be
done using the same basic circuit. In order to standardise the
heater and the thermometer currents, standard resistors of
100 $\Omega$ $\pm$ 0.005% and 10,000 $\Omega$ $\pm$ 0.005% values were used in the
respective circuits. Current value of 1$\mu$ A in the thermometer
circuit was controlled through a six step 0-1M$\Omega$ decade resistance
box. For the heater circuit a seven step 0-1 M$\Omega$ decade resis-
tance was necessary for proper heater current control. By changing
the variable resistors in the decade boxes, the potential drops
across the standard resistors were balanced against the chosen
fixed e.m.f. produced at the auxiliary binding posts of the K-3
potentiometer. Since the value of e.m.f. at the auxiliary binding
posts and the value of the standard resistors were known, it was
possible to know the exact values of current flowing in the
heater or the thermometer circuit. As the resistance of the
carbon thermometer, and thus the measuring current, changed
rapidly during the specific heat measurement, manual manipulation
of the adjustable resistor in the thermometer circuit was
necessary to return the measuring current to its desired value.
The heater resistance at liquid He temperature was also deter-
mined in each experiment with the help of the K-3 potentiometer.
In order to make the temperature measurements fast and continuous
during a heating cycle, the e.m.f. across the thermometer was
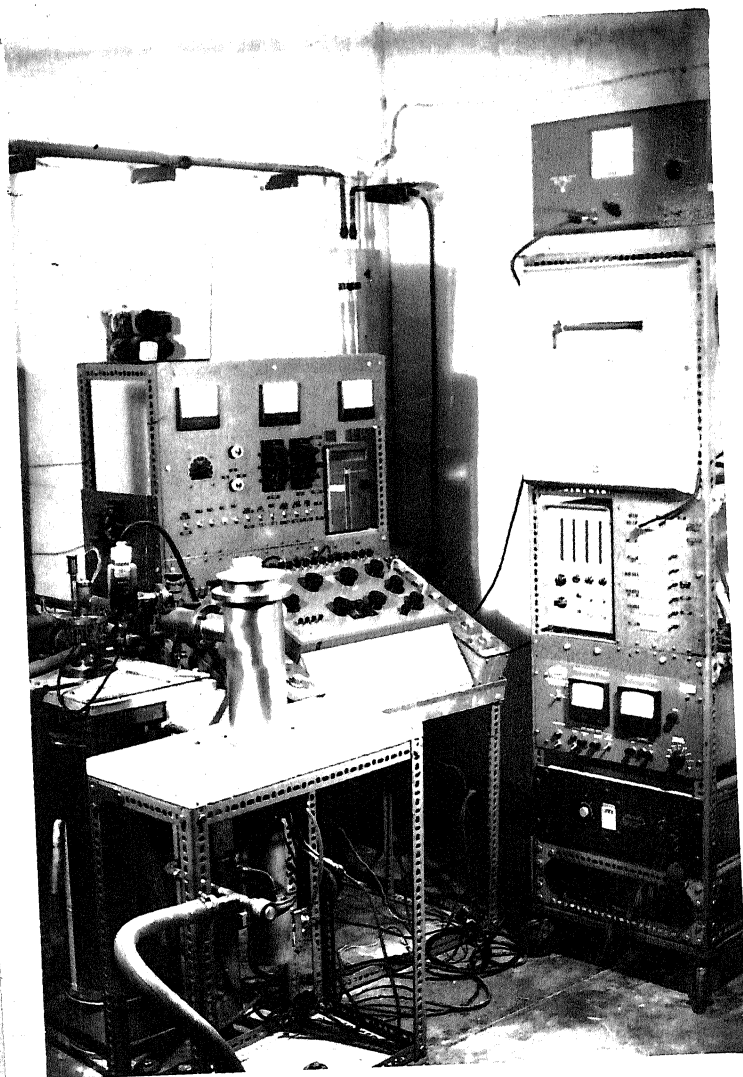
Fig.5: Photograph of the Apparatus and the Control Panel.

Fig.5:  Photograph of the Apparatus and the
        Control Panel.

slightly over balanced using the e.m.f. of the K-3 potentiometer. The difference e.m.f. was fed to a Leeds and Northrup D.C. microvolt amplifier (maximum output 10 mV, output characteristics linear), and the amplified e.m.f. was recorded on a Leeds and Northrup speedomax recorder at a chart speed of 3" per minute. The e.m.f. across the thermometer before the heating current was turned on and after it was turned off were recorded in this way, so that the change in the thermometer e.m.f. due to a heat pulse could be read directly and accurately from the chart. This change in e.m.f. could be readily converted into the temperature increment from the thermometer calibration data.

(b) <u>Time Measurement</u>:

A Beckman electronic E. Put and Timer (Model 5320) with maximum resolution of $10^{-4}$ seconds was used to accurately measure the duration of a heating period. In order to measure the duration of a heat pulse accurately, the heater switch and the timer were coupled so as to operate them simultaneously. This was achieved by opening the earth connection of the gate tube of the timer. The gate could be grounded via. the toggle switch $T_2$ (Figure 4) in the heater circuit. The switch $T_2$ at 'on' position completed the gate circuit as well as the heater circuit and the counting started. At 'off' position it 'opened' the gate circuit and the counting stopped. Therefore, the time interval for which $T_2$ was at 'on' position and hence the time for which the heater was on could be known accurately.

(c) <u>Accessory Equipments</u>: .

Several accessory equipments besides the main ones were incorporated in the electrical circuit. To take care of the large fluctuations in the line voltage a General Radio voltage regulator (model 1581 A H: regulations $\pm$ 10%; 4.6 kVA) was used for meeting the power requirements of all the instruments. A Veeco gauge control, (Type RG-31X) with provisions for use with two thermocouple gauges and one ionisation gauge inputs, was used to monitor vacuum at various parts of the apparatus. Two Leeds and Northrup constant voltage sources (2 Volts constant, 12 mA maximum) connected in parallel were used as the K-3 potentiometer power supplies. A third such constant voltage source was used in the thermometer circuit. Heater current was drawn from a 6 volt storage cell of low discharge characteristics.

Table 1 gives the list of the important equipments used together with their ranges, accuracy, capacity and any other important specifications. The circuit was designed keeping in view the low levels of currents and voltages involved. To eliminate stray e.m.f s the following precautions were taken:

(i)     the passive equipments, namely the K-3 potentiometer, the variable and the standard resistors, the galvanometer were mounted in one rack separate from the other housing the active equipments, namely the D.C. microvolt amplifier, the recorder, the counter and the vacuum gauge control,

(ii)    all connections were made with lacquered copper wires,

(iii)   necessary shieldings and groundings were made,

(iv)     thermal free solder was used for D.C. microvolt ampli-
fier and recorder connections,

(v)     the lead wires from the calorimeter to the measuring
panel were shielded and the shields properly grounded,

(vi)     the guarded circuits of the K-3 potentiometer were extended
to the external electrical circuit in the control panel.

With these precautions the electrical circuit rendered reliable
trouble free performance.

The potentiometer measured quantities  together with the
calibration data, recorded curves and the registered time provided
the necessary informations which had to be collected.  The experi-
mental  procedure, the method to obtain original data and the
calculations involved in deriving the final data are discussed
in subsequent chapters.

Table 1:  Instruments Used in the Electrical Circuit.

| Instrument | Model/Type | Specification | Supplier |
|---|---|---|---|
| Potentiometer | K-3 | Accuracy $\pm (0.015\% + 0.5 \mu V)$ | Leeds and Northrup Co. |
| Amplifier | No. 9835-A Stabilised D.C. | Accuracy $\pm (0.4\%$ of the amplifier range $+ 0.5 \mu V)$ | Leeds and Northrup Co. |
| Recorder | Speedomax Type G Model S | | Leeds and Northrup Co. |
| Counter | Beckman Model 5230 Universal E.Put and Timer. | Resolution 100 $\mu$ Sec. | Beckman Instruments Inc. |
| Galvanometer | No. 2430 | Sensitivity 0.0005 $\mu$ A/mm | Leeds and Northrup Co. |
| Standard Cell | Eppley | 1.01925 V at 23°C | Leeds and Northrup Co. |
| Standard Resistors | 100 ohm N.B.S. Type 10000 ohm N.B.S. Type | Accuracy $\pm 0.005\%$ at 25°C | Leeds and Northrup Co. |
| Power Resistors | Decade Box (i) Type 510 (ii) Type 1432-B | Range (i) 0-1 ohm (ii) 0-1 M ohm | General Radio Co. |
| Vacuum Gauge Control | Type RG-31X | Ranges (i) $1 \mu$ to 1 atm (ii) $10^{-4}$ torr to $10^{-10}$ torr | Vacuum Engineering and Electronics Co. |
| Voltage Regulator | Type 1581-AH | Correction range 230 V $\pm 10\%$ | General Radio Co. |
| Constant Voltage Supplies | No. 9879 | 2 Volts $\pm 0.3\%$ at 12.10 mA. | Leeds and Northrup |

# CHAPTER III

## EXPERIMENTAL PROCEDURE

### 3.1 Preparation of Specimen:

Specimen preparation consisted of alloy melting, annealing, metallographic examinations and finally machining into necessary shape and size.

### 3.1.1 Melting:

One binary Cr-Si alloy and nine ternary Cr-Fe-Si alloys were prepared. Taking the melting point of the binary Cr-Fe alloys as guide line, choice was made between the two available melting methods, namely, (i) electric arc melting, and (ii) induction melting in recrystallised alumina crucible. In both the cases a protective atmosphere of argon gas was used. The $Cr_{48.5} Fe_{48.5} Si$ alloy and two other alloys with higher Fe concentration were melted in induction furnace. Rest of the alloys including the binary Cr-Si alloy were melted in arc furnace. The amount of charge was limited to about 0.75 moles. This was a compromise between the necessity of larger specimens for better accuracy of measurement and the limitation due to the calorimeter size. In the induction furnace the complete charge could be melted into a single button. The arc furnace crucible could handle a maximum charge of about 25 gms. Because of this limitation two buttons had to be made for each arc melted alloy. Each alloy button was remelted at least twice, turning it upside down each time. By careful standardi- sation of the arc furnace parameters like current and time, the

melting losses could be kept to within 1% of the total charge. In induction melting the weight loss remained within 0.2%. All alloys were analysed chemically and the chemical compositions are shown in Table 2.

### 3.1.2   Heat Treatment:

After melting each alloy was given a homogeneous annealing treatment at suitable temperatures.   Since the specimen size was too large for sealing in evacuated silica capsule, they were annealed in a furnace with purified argon gas atmosphere. The specimens were wrapped in Mo foil, which acted as getter, for annealing in the gas furnace.   With adequate flushing of the furnace with argon gas prior to raising the temperature of the specimen  it was possible to prevent oxidation of the samples. To arrive at the appropriate annealing temperature $Cr_{92.15} Fe_{4.85} Si_3$ alloy was annealed at $1100^oC$ for 3 days and $Cr_{87.30} Fe_{9.70} Si_{3.00}$ alloy at $1150^oC$ for the same period of time.   Both showed small amounts of a second phase.   Subsequent annealing of these alloys at $1200^oC$ produced single phase alloys.   The annealing time and temperature used for various alloys are listed in Table 3.

### 3.1.3   Metallographic Examination:

The arc melted alloys were ground into approximate hemi spherical shapes and their flat surfaces were polished through 4/0 emery papers followed by finer polishing on wet cloth. The induction melted alloys were cut into two pieces and the flat surfaces were polished in the same manner. 5% Nital was used for $Cr_{4.85} Fe_{92.15} Si_{3.00}$ alloy as etchant.   All the other alloys

were electro etched using 10% oxalic acid as electrolyte and stainless steel as cathode. Examination of each sample showed that they were single phase alloys.

## 3.2 Experimental Operations:

The experimental operations may be divided into four major stages:

(i) specimen loading,

(ii) preliminary work,

(iii) calibration of carbon thermometer, and

(iv) recording of the heating curves.

## 3.2.1 Specimen Loading:

For specimen changing, the calorimeter assembly was mounted vertically in a stand. The calorimeter can was dismounted from its cover by melting down the Wood's metal joining the two. After demounting the can the lead wires from the heater and the thermometer were disconnected from the octal Kovar plug situated below the calorimeter cover. The specimen, hanging freely from a thread was cut loose. The calorimeter was then ready for mounting a new specimen.

The specimen, in two pieces, was weighed and placed on the two opposite faces of the heater-thermometer assembly (Figure 3). A very thin film of high vacuum silicon grease was applied to the contact surfaces for good thermal contact between the specimen and the heater-thermometer assembly. Bare 26 gauge copper wire was used to rigidly tie the specimen

## Table  2

## Chemical Composition of Alloy Specimens

| Sl. No. | Nominal Compositions At% | | | Analysed Compositions At% | | |
|---|---|---|---|---|---|---|
| | Cr | Fe | Si | Cr | Fe | Si |
| 1. | 92.15 | 4.85 | 3.00 | 92.11 | 4.88 | 3.01 |
| 2. | 87.30 | 9.70 | 3.00 | 87.25 | 9.68 | 3.07 |
| 3. | 82.45 | 14.55 | 3.00 | 81.71 | 14.41 | 3.88 |
| 4. | 77.60 | 19.40 | 3.00 | 77.63 | 19.58 | 2.79 |
| 5. | 72.75 | 24.25 | 3.00 | 73.04 | 24.35 | 2.61 |
| 6. | 67.90 | 29.10 | 3.00 | 67.45 | 28.46 | 4.09 |
| 7. | 48.50 | 48.50 | 3.00 | 48.29 | 48.87 | 2.84 |
| 8. | 24.25 | 72.75 | 3.00 | 23.22 | 73.88 | 2.90 |
| 9. | 4.85 | 92.15 | 3.00 | 4.95 | 92.10 | 2.95 |
| 10. | 97.00 | – | 3.00 | 97.02 | – | 2.98 |

Table 3

Melting and Annealing History of the Alloy Specimens

| Sl. No. | Alloys with nominal compositions | Melting furnace | Annealing temperature* | Annealing time |
|---|---|---|---|---|
| 1. | $Cr_{92.15} Fe_{4.85} Si_{3.00}$ | Arc | $1100^{o}C$ <br> $1200^{o}C$ | 3 Days <br> 3 Days |
| 2. | $Cr_{87.30} Fe_{9.70} Si_{3.00}$ | Arc | $1150^{o}C$ <br> $1200^{o}C$ | 3 Days <br> 3 Days |
| 3. | $Cr_{82.45} Fe_{14.55} Si_{3.00}$ | Arc | $1200^{o}C$ | 3 Days |
| 4. | $Cr_{77.60} Fe_{19.40} Si_{3.00}$ | Arc | $1200^{o}C$ | 3 Days |
| 5. | $Cr_{72.75} Fe_{24.25} Si_{3.00}$ | Arc | $1200^{o}C$ | 3 Days |
| 6. | $Cr_{67.90} Fe_{29.10} Si_{3.00}$ | Arc | $1200^{o}C$ | 3 Days |
| 7. | $Cr_{48.50} Fe_{48.50} Si_{3.00}$ | Induction | $1200^{o}C$ | 3 Days |
| 8. | $Cr_{24.25} Fe_{72.75} Si_{3.00}$ | Induction | $1200^{o}C$ | 3 Days |
| 9. | $Cr_{4.85} Fe_{92.15} Si_{3.00}$ | Induction | $1100^{o}C$ <br> $800^{o}C$ | 2 Days <br> 3 Days |
| 10. | $Cr_{97.00} Si_{3.00}$ | Arc | $1300^{o}C$ | 3 Days |

* The higher annealing temperature for some of the alloys, except the alloy no. 9, indicates the final annealing tempe- rature from which they were quenched. The alloy no. 9 was quenched from $800^{o}C$.

to the heater-thermometer assembly for holding the pieces together
and for better thermal contact between the specimen and the
heater-thermometer assembly. The assembly was reweighed to
determine the total amount of copper in the specimen-heater-
thermometer assembly. Before mounting the specimen in the
calorimeter it was found important to carefully inspect the
tinned lip of the calorimeter can. Any sticky material,
usually oxide, formed during the demounting operations had to
be carefully removed to ensure a dependable joint. A simple
way for its removal was to use a jeweller's file, or even a
safety razor blade. In the case of a very extensive film for-
mation it was found advisable to completely clean the surface
with coarse and subsequently fine emery papers, or with proper
care by a jeweller's file, and re-tin it. The same procedure
was adopted for the calorimeter can top onto which the calori-
meter can was soldered. Since this was the most vulnerable of
all the vacuum joints and had to be handled in every experiment,
a detailed procedure for obtaining a dependable joint is given
in the Appendix A.

The specimen was suspended with a thread at the calori-
meter centre in such a manner that it did not touch the can wall.
The lead wires were soldered to the appropriate pins in the
octal Kovar plug. Before the calorimeter can was mounted the
resistance values of the lead wires were measured as a check
against any short circuiting between the lead wires themselves
and also between the lead wires and the calorimeter body. After

this routine check the calorimeter can was pushed onto the cover and soldered with Wood's metal.

Before putting the calorimeter assembly in the cryostat it was essential to make vacuum check. For this the calorimeter assembly was coupled with the vacuum train (Figure 2) outside the cryostat and evacuated. The freshly made Wood's metal joint was carefully tested for leak. Sometimes a joint found irreproachable at room temperature showed leak at liquid He temperature. To take precautions against such a low temperature leak (different from superfluid leak) the calorimeter can, when at about $1 \times 10^{-5}$ torr. pressure, was dipped in liquid nitrogen. If the vacuum stayed it was found that the joint was leak proof at liquid He temperature.

## 3.2.2 Preliminary Work:

The calorimeter assembly after specimen loading and vacuum checking, was assembled in the cryostat and coupled with the vacuum train. The calorimeter was evacuated to a high vacuum ( $1 \times 10^{-5}$ torr.). The inside and also the space between the double walls of the He dewar were evacuated to a pressure of about $4 \times 10^{-2}$ torr. Next the mechanical pump (Mech. Pump No.2, Figure 2) used for the purpose was put off and the valves $V_8$ and $V_{11}$ (Figure 2) closed. By opening valve $V_9$ a small amount of air was allowed to leak into the He dewar jacket. When this air pressure was about 0.5 to 1.0 torr. the valve $V_{10}$ was closed Liquid nitrogen was transferred from the storage dewar through

a syphon till the experimental nitrogen dewar was filled almost to the brim. After liquid nitrogen filling the He dewar was filled with dry He gas from a gas cylinder to one atmosphere pressure. This gas acted as heat exchanger for cooling the calorimeter assembly to liquid nitrogen temperature. About 1 mm Hg of He gas was then introduced into the calorimeter through the valve $V_{14}$ to act as an exchange gas between the calorimeter can and the specimen. The system was left overnight, 8 to 10 hrs, to come down to liquid $N_2$ temperature.

Before starting liquid He transfer, liquid nitrogen in the nitrogen dewar was replenished. Then a routine check of the heater and the thermometer resistances was made to ascertain that the system reached liquid $N_2$ temperature. The vacuum space of the He transfer tube was evacuated to about $4 \times 10^{-2}$ torr. A puff of He gas from the cylinder was allowed through the liquid He transfer tube to make sure that the passage was free. Before bringing the He storage dewar the valve $V_2$ (Figure 2) in the recovery line was opened such that the evaporated He gas could escape to the He gas bag for collection and subsequent recirculation. The storage dewar was brought into the room and its bleeder outlet was connected to the valve $V_{11}$ (Figure 2) in the experimental He dewar top. The storage dewar was allowed to rest for a few minutes for stabilising the gas pressure inside it. The liquid He transfer tube was connected to the He gas cylinder and its two ends inserted into the storage and the experimental dewars. The valve $V_{11}$ (Figure 2) was closed and

the transfer tube slowly pushed inside the storage and the experimental dewars, taking precaution against sudden pressure rise. When the transfer tube was lowered at a correct rate no over pressure was found necessary for the liquid He transfer. Sometimes only, about 1/4 to 1/2 psi over pressure was necessary for the transfer. When the liquid started flowing into the dewar, its level inside was followed. With about 3/4th of the dewar filled, the bleeder outlet of the storage dewar was opened by opening the valve $V_{11}$ (Figure 2), to release the gas pressure inside it, and the transfer tube was raised above the liquid level of the storage dewar thus stopping any further liquid flow. After allowing the storage dewar pressure to come down to about the normal atmospheric pressure, the transfer tube was taken out and the storage dewar and the He intake tube of the experimental dewar were closed by the respective stoppers, and then valve $V_{11}$ was closed. After liquid He transfer, the potentiometer current was standardised and the heater and the thermometer resistance values were measured and noted down. The thermometer current was standardised at $1 \mu A$ value by appropriately setting the decade resistance in the thermometer circuit (Figure 4). Next the heating currents were standardised for 0.1, 0.2, 0.3, 0.5, 0.8, and 1.0 mA values by adjusting the two variable resistors in the heater circuit (Figure 4). Also the microvolt amplifier and the recorder were calibrated using the calibrated e.m.f. from the K-3 potentiometer. Finally the switches were set at recording position.

The switch positions for various operations are shown in the Appendix B.

### 3.2.3 Thermometer Calibration:

The carbon thermometer was calibrated against the temperature of the liquid He bath, as determined from the vapour pressure at the surface of the liquid He bath, using 1958 N.B.S. $He^4$ scale of temperature. Before pumping over liquid He to lower the vapour pressure, the valve $V_2$ (Figure 2) in the recovery line was closed and the valve $V_3$ in the pumping line was opened. The valves $V_4, V_5$ and $V_{17}$ were kept closed for a few minutes to allow the He bath and the pressure over it to come to a steady state condition. Gradually the pumping rate was increased by opening the appropriate valves $V_{17}, V_4$ and $V_5$. The manometer pressure was read by the cathetometer and the corresponding e.m.f. developed across the thermometer was noted.

Since the measuring current of the thermometer was fixed at $1\mu A$ in the start of the experiment, during calibration of the thermometer as the temperature reduced and the thermometer resistance increased a corresponding decrease in the external circuit resistance was made to keep the measuring current constant. By keeping the measuring current constant at $1\mu A$, the potential across the thermometer in $\mu V$ could be directly converted into its resistance value. In order to get a good calibration curve about 8 to 10 readings above the $\lambda$ transition temperature and 4 to 5 readings below it were taken.

### 3.2.4 Recording:

After completing the thermometer calibration, the valves $V_3$, $V_4$, $V_5$ (Figure 2) in the pumping line were opened and the He bath was allowed to come down to the lowest possible temperature. When the He bath pressure attained a steady state, as indicated by the thermometer resistance value, the calorimeter was evacuated to remove the exchange gas and bring about the thermal isolation of the specimen. Diffusion pump was started after running the mechanical pump for a few minutes and the cold trap over the diffusion pump was filled with liquid nitrogen. In about 40-45 minutes a vacuum of the order of $4 \times 10^{-6}$ torr. could be obtained in the vacuum line joining the cold trap and the calorimeter. However, since the calorimeter can remained dipped in the liquid He bath, actual vacuum inside it is expected to be of higher order than measured outside at room temperature making the system essentially adiabatic.

Before starting the heating cycle of the specimen, the potentiometer was standardised and the thermometer current was reset at $1\mu A$. The recording sequence of the heating curve was the following:

(i) The timer was reset and the heater circuit resistance was adjusted to get the appropriate heater current.

(ii) The chart motor of the recorder was started and the thermal drift was traced for about 1 to 2 minutes,

(iii) Heating current and also the heating steps (set approximately at $0.1^\circ k$ apart at temperatures higher

than $2^O$k) were selected properly depending upon the specimen temperature,

(iv)   The heater was energised till the thermometer resistance changed approximately by the amount desired and the thermometer circuit resistance was adjusted to keep the measuring current constant,

(v)    The heater current was put off,

(vi)   The timer was reset after noting the heating time,

(vii)  The thermal drift was traced for about 1 to 2 minutes.

Same procedure was repeated for subsequent recordings. About 30 to 40 readings were taken in the temperature range of $1.4^O$K to $4.2^O$K. A typical heating curve is shown in Figure 6.

In the exchange gas calorimeter the adsorbed gas from the specimen (and possibly from the calorimeter) released during the heating periods sometimes introduced some thermal drift. When the drift became appreciable, as indicated by the preheating recorder trace, the specimen was 'baked' by closing all the valves in the pumping line, so that the bath warmed up a little, thereby helping evolution of the adsorbed gas. Baking was continued till the thermal drift became very small. Several such bakings during the entire period gave satisfactory heating curves without any appreciable thermal drift.

The trace of the heating curve, the K-3 potentiometer readings, the heater and the thermometer current values, the heater resistance, the heating period as registered in the timer,

together with the thermometer calibration data provided all the necessary informations for calculating the specific heat values. The actual method of calculating the specific heat C from these data is given in the Appendix C.

# CHAPTER IV

## RESULTS

### 4.1 Experimental Errors:

The thermometer calibration is an important part of the experimental work, and the accuracy of the final result depend on the accuracy of its calibration. The resistance temperature relationship of the carbon resistor thermometers used could be satisfactorily represented at the liquid He temperatures by the expression[44].

$$(\text{Log} \, R/T)^{1/2} = A + B \, \text{Log} \, R \qquad (4.1)$$

where A and B are constants. The constants A and B for the thermometers were determined by the method of least squares, using the calibration data. The accuracy of the calibration of the thermometer was estimated to be better than $\pm 0.001^\circ k$.

Generally, the experimental errors may be classified into:

(a) Random errors which include the personal errors, and

(b) the instrumental errors and the systematic errors.

The random errors can be minimised by the least squares technique for a large number of observations, but the systematic errors are difficult to evaluate.

The instrumental errors are listed in Table 4, together with the critical measured quantities and the estimated percentage

errors of the quantities $i, R, t, n_s$ and $\triangle T$; where $i$ and $R$ are the heating current and the heater resistance respectively, $t$ the duration of a heat pulse, $n_s$ the number of moles of the specimen and $\triangle T$ the temperature increment due to a heat pulse. The total instrumental error introduced in $C/T$ was estimated to be within $\pm 1\%$ of which more than $90\%$ was caused by the error in measuring the temperature rise during a heat pulse.

The major part of the systematic error originated from the estimation of the heater resistance $R_H$. The change in $R_H$ from 1.4 to $4.2\,^{\circ}k$ was only $0.2\,\Omega$ or $0.07\%$. However, about 3/4" long pieces of Manganin wire were used to connect the heater coil to the junction points of the current and potential lead wires located at the Kovar plug in the calorimeter. An estimation of the amount of heat dissipated in these two sections when heating current passed through these sections was difficult. It was assumed that one half of the heat went to the specimen, while the other half went to the calorimeter. Accordingly, the following expression, as suggested by Cheng[45], was used for all calculations:

$$R_H = \frac{1}{2}(R_{4.2} + R_{1.4}) - 2\,\Omega \qquad (4.2)$$

Here $R_H$ is the 'effective resistance' of the heater coil, $R_{4.2}$ and $R_{1.4}$ are the measured resistance values at $4.2\,^{\circ}k$ and $1.4\,^{\circ}k$ of the heater coil including both the connecting wires, $2\,\Omega$ is the resistance of one of the connecting wires.

Table 4:  List of instrumental errors entering into the final results

| Instrument | Accuracy | Critical Measured Quantity | Max. ± Percentage Error in | | | | |
|---|---|---|---|---|---|---|---|
| | | | $I$ | $R_H$ | $t$ | $n$ | $T$ |
| K-3 | ±(0.015% +0.5μV) | 0.2 mA | 0.018 | 0.016 | | | 0.027 |
| Std.Cell and | ± 0.01% | 100 ohms | 0.015 | | | | |
| Std.Resistor | ± 0.005% | 300 ohms | | 0.015 | | | 0.003 |
| | | 10,000 ohms at 100 X | | | | | |
| Counter | 100 μSec. | ~20 Sec. | | | 0.0005 | | |
| Balance | 0.00005 gm | ~40 gms. | | | | 0.00013 | |
| Amplifier and Recorder | ±(0.4% of Amplifier range +0.5μV) | 100 X | | | | | 0.027 |
| | | Total: | 0.033 | 0.031 | 0.0005 | 0.00013 | 0.057 |

4.2  Specific Heat Data:

The low temperature specific heat of metals and alloys can be expressed by the two parameter equation $C = \gamma T + \beta T^3$ (equation 1.1), $\gamma$ is the intercept and $\beta$ the slope of the straight line obtained by plotting $C/T$ as a function of $T^2$. To minimise the random errors, $\gamma$ and $\beta$ were calculated in the present work by the least squares method.

(a)  Copper:

The specific heat data of copper are listed in Table 5 and plotted as $C/T$ vs. $T^2$ in Figure 8. Low temperature specific heat of Cu has been studied by several workers. The results obtained from the present work are: $\gamma = 1.667 \times 10^{-4}$ cal.mol$^{-1}$ deg.$^{-2}$, $\beta = 0.1172$ cal.mol.$^{-1}$ deg.$^{-4}$ and $\theta_D = 341^\circ$K. The agreement between the present work and the previous results[46] is quite satisfactory.

(b)  $Cr_{97} Si_3$:

The specific heat data for the binary $Cr_{97} Si_3$ alloy is given in Table 6 and plotted in $C/T$ vs. $T^2$ in Figure 9. The specific heat data of this binary alloy has a normal straight line behaviour as in anti-ferromagnetic Cr. However, the $\gamma$ calculated from the data has a larger value than that of pure anti-ferromagnetic Cr.[20]

(c) Ternary Cr-Fe-Si Alloys:

Nine ternary alloys of $(Cr_x Fe_{1-x})_{97} Si_3$ were investigated. The specific heat data for these alloys are given in Tables 7 to 15, and $C/T$ vs. $T^2$ plots are shown in Figures 9 to 13. The $C/T$ vs. $T^2$ plot for the alloys $Cr_{92.15} Fe_{4.85} Si_{3.00}$, $Cr_{82.45} Fe_{14.55} Si_{3.00}$, $Cr_{77.60} Fe_{19.40} Si_{3.00}$, $Cr_{72.75} Fe_{24.25} Si_{3.00}$, $Cr_{67.90} Fe_{29.10} Si_{3.00}$ show up-turn effect. Such up-turn effect has been reported[47] in alloys with critical compositions for non ferromagnetic to ferromagnetic transitions, and is attributed to contributions to specific heat from super paramagnetic clusters formed in such alloys. The specific heat data for these alloys showing anomolous behaviour are represented by the three parameter equation,

$$C = A + \gamma T + \beta T^3 \qquad (4.3)$$

where A is a temperature independent contribution from the super paramagnetic clusters. According to this equation the $(C-A)/T$ plot as a function of $T^2$ is expected to be a straight line. The $(C-A)/T$ vs. $T^2$ plots for the alloys $Cr_{92.15} Fe_{4.85} Si_{3.00}$, $Cr_{82.45} Fe_{14.55} Si_{3.00}$, $Cr_{77.60} Fe_{19.40} Si_{3.00}$, $Cr_{72.75} Fe_{24.25} Si_3$, $Cr_{67.90} Fe_{29.10} Si_{3.00}$ are shown in Figures 14 and 15. The data points fall reasonably well on straight lines. All the curves except that of $Cr_{92.15} Fe_{4.85} Si_{3.00}$ have positive slope. For this alloy with negative $\beta$ value, $\gamma$ has been estimated by extrapolation of high temperature data in $C/T$ vs. $T^2$ plot.

The alloy $Cr_{87.30}$ $Fe_{9.70}$ $Si_{3.00}$ has a C/T vs. $T^2$ plot, as shown in Figure 10, which droops down wards at lower temperatures. To check if this is due to some spurious effects the experiment was repeated. The data points of two separate experiments, shown by filled and open circles in the Figure 10, fall on the same curve, thus indicating that the anomaly is truly due to material properties. Such anomaly in C/T vs. $T^2$ plot has been earlier reported[31] in $Fe_{65}Al_{35}$ alloy and was thought to be due to its complex magnetic structure.

For the rest of the alloys, $Cr_{48.5}$ $Fe_{48.5}$ $Si_{3.00}$, $Cr_{24.25}$ $Fe_{72.75}$ $Si_{3.00}$, $Cr_{4.85}$ $Fe_{92.15}$ $Si_{3.00}$ the C/T vs. $T^2$ plots, shown in Figures 12 and 13, are well behaved straight lines, from which values of $\gamma$ and $\beta$ could be easily derived by the least squares fit.

The specific heat data including the values of A, $\gamma$, $\beta$, Debye temperature $\theta_D$ together with the root mean square deviation of C for all the alloys are listed in Table 16. For the alloy $Cr_{82.45}$ $Fe_{14.55}$ $Si_{3.00}$ which shows a droop in the C/T vs. $T^2$ plot the root mean square deviation has been calculated considering only those data points which fall on the straight line part of the curve.
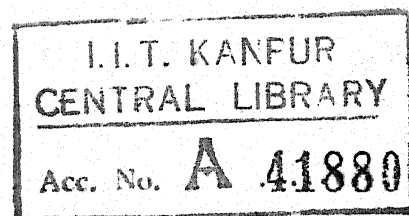
Table 5:   Specific Heat Data For Pure Copper

| $T$ ($^{\circ}K$) | $C$ (In $10^{-4}$ cal.mol.$^{-1}$deg.$^{-1}$) | $C/T$ (In $10^{-4}$ cal.mol.$^{-1}$deg.$^{-2}$) | $T^2$ ($^{\circ}K^2$) |
|---|---|---|---|
| 1.7136 | 3.4980 | 2.0413 | 2.9364 |
| 1.9195 | 3.8783 | 2.0204 | 3.6845 |
| 1.9794 | 4.3069 | 2.1758 | 3.9180 |
| 2.1160 | 4.6745 | 2.2091 | 4.4774 |
| 2.1967 | 4.9418 | 2.2496 | 4.8255 |
| 2.2568 | 5.1193 | 2.2683 | 5.0931 |
| 2.3702 | 5.4544 | 2.3012 | 5.6178 |
| 2.4922 | 5.8664 | 2.3539 | 6.2111 |
| 2.5764 | 6.3122 | 2.4500 | 6.6378 |
| 2.6529 | 6.7263 | 2.5354 | 7.0379 |
| 2.7283 | 7.0837 | 2.5963 | 7.4436 |
| 2.8102 | 7.2771 | 2.5895 | 7.8467 |
| 2.8165 | 7.4458 | 2.6436 | 7.9327 |
| 2.8825 | 7.4660 | 2.5901 | 8.3088 |
| 2.8989 | 7.8609 | 2.7116 | 8.4036 |
| 2.9089 | 7.5811 | 2.6061 | 8.4617 |
| 2.9635 | 7.7924 | 2.6294 | 8.7823 |
| 3.0167 | 8.4040 | 2.7858 | 9.1005 |
| 3.0362 | 8.3903 | 2.7634 | 9.2185 |
| 3.1660 | 8.8642 | 2.7998 | 10.0235 |
| 3.1720 | 6.6343 | 2.7220 | 10.0616 |
| 3.3201 | 9.9416 | 2.9943 | 11.0231 |
| 3.4326 | 10.4441 | 3.0426 | 12.1375 |
| 3.6283 | 11.9015 | 3.2801 | 13.1646 |
| 3.7469 | 12.7238 | 3.3958 | 14.0393 |

Table 6: Specific Heat Data for $Cr_{97}Si_3$

| T ($^\circ$K) | C (in $10^{-4}$ cal.mol.$^{-1}$ deg.$^{-1}$) | C/T (in $10^{-4}$ cal.mol.$^{-1}$deg.$^{-2}$) | $T^2$ ($^\circ$K$^2$) |
|---|---|---|---|
| 1.349 | 8.66 | 6.42 | 1.822 |
| 1.357 | 8.68 | 6.40 | 1.842 |
| 1.428 | 9.00 | 6.30 | 2.039 |
| 1.507 | 9.74 | 6.46 | 2.272 |
| 1.515 | 9.46 | 6.24 | 2.296 |
| 1.572 | 9.81 | 6.24 | 2.471 |
| 1.579 | 10.16 | 6.44 | 2.494 |
| 1.637 | 10.17 | 6.22 | 2.679 |
| 1.640 | 10.37 | 6.32 | 2.689 |
| 1.719 | 10.74 | 6.25 | 2.955 |
| 1.724 | 11.06 | 6.41 | 2.973 |
| 1.831 | 11.57 | 6.32 | 3.352 |
| 1.832 | 11.77 | 6.42 | 3.355 |
| 1.909 | 12.00 | 6.29 | 3.644 |
| 1.980 | 12.60 | 6.36 | 3.920 |
| 2.057 | 13.18 | 6.41 | 4.231 |
| 2.140 | 13.59 | 6.35 | 4.579 |
| 2.228 | 14.26 | 6.40 | 4.962 |
| 2.363 | 15.16 | 6.42 | 5.584 |
| 2.397 | 15.23 | 6.40 | 5.659 |
| 2.470 | 15.92 | 6.45 | 6.100 |
| 2.499 | 16.12 | 6.45 | 6.245 |
| 2.593 | 16.81 | 6.48 | 6.722 |
| 2.614 | 16.78 | 6.42 | 6.832 |
| 2.737 | 17.84 | 6.52 | 7.492 |
| 2.741 | 17.71 | 6.46 | 7.514 |
| 2.923 | 19.08 | 6.53 | 8.542 |
| 3.176 | 21.18 | 6.67 | 10.009 |
| 3.391 | 22.64 | 6.68 | 11.496 |
| 3.611 | 24.67 | 6.83 | 13.038 |
| 3.818 | 25.26 | 6.88 | 14.574 |
| 3.985 | 27.70 | 6.95 | 15.883 |
| 4.167 | 29.29 | 7.03 | 17.363 |
| 4.372 | 31.70 | 7.25 | 19.111 |

Table 7: Specific Heat Data for $Cr_{92.15}Fe_{4.85}Si_{3.00}$

| T (°K) | C (In $10^{-4}$ Cal. mol.$^{-1}$deg.$^{-1}$) | C/T (In $10^{-4}$ Cal. mol.$^{-1}$deg.$^{-2}$) | (C-A)/T (In $10^{-4}$ Cal. mol.$^{-1}$deg.$^{-2}$) | $T^2$ (°K$^2$) |
|---|---|---|---|---|
| 1.259 | 33.22 | 26.38 | 19.38 | 1.586 |
| 1.302 | 33.94 | 26.06 | 19.29 | 1.696 |
| 1.352 | 35.25 | 26.07 | 19.55 | 1.828 |
| 1.398 | 36.11 | 25.84 | 19.52 | 1.953 |
| 1.404 | 36.11 | 25.72 | 19.44 | 1.970 |
| 1.435 | 37.04 | 25.82 | 19.67 | 2.058 |
| 1.484 | 37.55 | 25.30 | 19.35 | 2.203 |
| 1.514 | 37.88 | 25.02 | 19.19 | 2.293 |
| 1.555 | 39.13 | 25.17 | 19.49 | 2.417 |
| 1.622 | 40.78 | 25.13 | 19.70 | 2.633 |
| 1.688 | 41.65 | 24.67 | 19.44 | 2.850 |
| 1.767 | 43.68 | 24.12 | 19.72 | 3.122 |
| 1.910 | 46.15 | 24.16 | 19.54 | 3.649 |
| 1.978 | 47.51 | 24.03 | 19.56 | 3.911 |
| 2.069 | 49.77 | 24.06 | 19.79 | 4.280 |
| 2.194 | 52.08 | 23.73 | 19.71 | 4.816 |
| 2.297 | 53.89 | 23.45 | 19.62 | 5.278 |
| 2.342 | 55.16 | 23.55 | 19.78 | 5.486 |
| 2.397 | 55.97 | 23.35 | 19.67 | 5.744 |
| 2.469 | 57.52 | 23.30 | 19.72 | 6.069 |
| 2.472 | 56.81 | 22.98 | 19.42 | 6.112 |
| 2.580 | 58.90 | 22.83 | 19.42 | 6.657 |
| 2.585 | 59.38 | 22.97 | 19.55 | 6.681 |
| 2.721 | 61.45 | 22.58 | 19.35 | 7.406 |
| 2.726 | 62.43 | 22.90 | 19.66 | 7.431 |
| 2.758 | 62.68 | 22.72 | 19.52 | 7.609 |
| 2.907 | 64.90 | 22.33 | 19.29 | 8.450 |
| 3.168 | 69.61 | 21.97 | 19.18 | 10.036 |
| 3.421 | 73.85 | 21.59 | 19.45 | 11.703 |
| 3.699 | 76.55 | 21.21 | 18.83 | 13.022 |
| 3.841 | 82.32 | 21.43 | 19.13 | 14.756 |
| 4.191 | 89.47 | 21.35 | 19.24 | 17.563 |
| 4.367 | 93.13 | 21.34 | 19.30 | 19.068 |

Table 8a: Specific Heat Data for $Cr_{87.30} Fe_{9.70} Si_{3.00}$.

| T ($^{\circ}K$) | C (In $10^{-4}$ Cal. mol.$^{-1}$ deg.$^{-1}$) | C/T (In $10^{-4}$ Cal. mol.$^{-1}$ deg.$^{-2}$) | $T^2$ ($^{\circ}K^2$) |
|---|---|---|---|
| 1.710 | 49.88 | 42.60 | 1.371 |
| 1.191 | 50.88 | 42.72 | 1.419 |
| 1.213 | 52.21 | 43.02 | 1.472 |
| 1.238 | 53.02 | 42.83 | 1.532 |
| 1.388 | 60.25 | 43.40 | 1.927 |
| 1.443 | 62.67 | 43.44 | 2.082 |
| 1.477 | 64.12 | 43.41 | 2.182 |
| 1.627 | 71.94 | 44.30 | 2.637 |
| 1.710 | 75.32 | 44.05 | 2.924 |
| 1.828 | 80.92 | 44.25 | 3.343 |
| 1.919 | 85.14 | 44.36 | 3.684 |
| 2.091 | 92.63 | 44.30 | 4.372 |
| 2.205 | 97.24 | 44.09 | 4.863 |
| 2.359 | 104.50 | 44.30 | 5.564 |
| 2.471 | 109.29 | 44.23 | 6.106 |
| 2.603 | 115.21 | 44.26 | 6.774 |
| 2.928 | 129.29 | 44.16 | 8.572 |
| 3.200 | 142.54 | 44.55 | 10.238 |
| 3.222 | 142.32 | 44.17 | 10.381 |
| 3.403 | 149.66 | 43.97 | 11.584 |
| 3.609 | 161.13 | 44.55 | 13.023 |
| 3.806 | 170.08 | 44.69 | 14.484 |
| 3.953 | 175.79 | 44.47 | 15.627 |
| 4.115 | 182.25 | 44.29 | 16.933 |
| 4.316 | 191.81 | 44.44 | 18.626 |

Table 8b: Specific Heat Data for $Cr_{87.30} Fe_{9.70} Si_{3.00}$

| $T$ ($^\circ k$) | $C$ (In $10^{-4}$ Cal. mol.$^{-1}$ deg.$^{-1}$) | $C/T$ (In $10^{-4}$ Cal. mol.$^{-1}$ deg.$^{-2}$) | $T^2$ ($^\circ k^2$) |
|---|---|---|---|
| 1.234 | 53.12 | 43.05 | 1.522 |
| 1.264 | 54.16 | 42.85 | 1.597 |
| 1.304 | 56.14 | 43.06 | 1.699 |
| 1.354 | 58.18 | 42.96 | 1.835 |
| 1.387 | 59.96 | 43.22 | 1.928 |
| 1.465 | 64.04 | 43.71 | 2.147 |
| 1.545 | 67.50 | 43.69 | 2.387 |
| 1.736 | 76.09 | 43.83 | 3.014 |
| 1.852 | 81.61 | 44.06 | 3.431 |
| 1.986 | 87.83 | 44.23 | 3.943 |
| 2.177 | 97.11 | 44.60 | 4.740 |
| 2.363 | 104.88 | 44.39 | 5.583 |
| 2.493 | 110.90 | 44.48 | 6.215 |
| 2.667 | 119.68 | 44.87 | 7.115 |
| 2.841 | 126.25 | 44.43 | 8.073 |
| 3.011 | 134.23 | 44.58 | 9.067 |
| 3.143 | 138.02 | 43.91 | 9.878 |
| 3.272 | 146.43 | 44.75 | 10.708 |
| 3.453 | 155.64 | 45.07 | 11.923 |
| 3.648 | 162.47 | 44.54 | 13.307 |
| 3.984 | 177.36 | 44.51 | 15.875 |

Table 9: Specific Heat Data for $Cr_{82.45}$ $Fe_{14.55}$ $Si_{3.00}$

| T ($^\circ$K) | C (In $10^{-4}$ Cal. mol.$^{-1}$ deg.$^{-1}$) | C/T (In $10^{-4}$ Cal. mol.$^{-1}$ deg.$^{-2}$) | (C-A)/T (In $10^{-4}$ Cal. mol.$^{-1}$ deg.$^{-2}$) | $T^2$ ($^\circ$K$^2$) |
|---|---|---|---|---|
| 1.289 | 69.91 | 54.21 | 42.90 | 1.663 |
| 1.327 | 70.21 | 52.89 | 41.90 | 1.762 |
| 1.357 | 71.88 | 52.96 | 42.20 | 1.842 |
| 1.423 | 73.22 | 51.46 | 41.19 | 2.024 |
| 1.462 | 76.59 | 52.39 | 42.39 | 2.137 |
| 1.565 | 81.04 | 51.77 | 42.45 | 2.450 |
| 1.693 | 85.17 | 50.30 | 41.68 | 2.867 |
| 1.842 | 93.09 | 50.53 | 42.61 | 3.394 |
| 1.988 | 98.78 | 49.69 | 42.34 | 3.952 |
| 2.169 | 105.89 | 48.81 | 42.08 | 4.707 |
| 2.440 | 119.03 | 48.78 | 42.80 | 5.955 |
| 2.684 | 129.78 | 48.35 | 42.91 | 7.203 |
| 2.783 | 134.13 | 48.19 | 42.95 | 7.743 |
| 2.890 | 139.73 | 48.34 | 43.29 | 8.354 |
| 2.997 | 144.34 | 48.16 | 43.29 | 8.982 |
| 3.057 | 146.13 | 47.80 | 43.02 | 9.345 |
| 3.246 | 154.57 | 47.62 | 43.12 | 10.535 |
| 3.411 | 162.61 | 47.67 | 43.39 | 11.636 |
| 3.511 | 168.11 | 47.88 | 43.72 | 12.325 |
| 3.572 | 169.34 | 47.41 | 43.32 | 12.759 |
| 3.692 | 173.56 | 47.01 | 43.05 | 13.629 |
| 3.798 | 180.96 | 47.64 | 43.80 | 14.422 |
| 3.920 | 187.10 | 47.73 | 44.00 | 15.365 |
| 4.050 | 195.07 | 48.16 | 44.56 | 16.405 |
| 5.261 | 203.12 | 47.67 | 44.24 | 18.158 |
| 4.416 | 210.80 | 47.74 | 44.43 | 19.501 |
| 4.596 | 219.85 | 47.84 | 44.66 | 21.122 |
| 4.760 | 228.72 | 48.04 | 44.98 | 22.663 |

Table 10:  Specific Heat Data for $Cr_{77.60}$ $Fe_{19.40}$ $Si_{3.00}$

| $T$ ($^{o}K$) | $C$ (In $10^{-4}$ Cal. mol.$^{-1}$ deg.$^{-1}$) | $C/T$ (In $10^{-4}$ Cal. mol.$^{-1}$ deg.$^{-2}$) | $(C-A)/T$ (In $10^{-4}$ Cal. mol.$^{-1}$ deg.$^{-2}$) | $T^2$ ($^{o}K^2$) |
|---|---|---|---|---|
| 1.352 | 59.95 | 44.35 | 38.89 | 1.827 |
| 1.469 | 64.83 | 44.14 | 39.11 | 2.157 |
| 1.628 | 70.90 | 43.56 | 39.02 | 2.650 |
| 1.694 | 74.07 | 43.72 | 39.36 | 2.871 |
| 1.764 | 77.03 | 43.67 | 39.48 | 3.111 |
| 1.852 | 81.27 | 43.87 | 39.88 | 3.432 |
| 1.935 | 85.11 | 43.99 | 40.17 | 3.743 |
| 2.004 | 86.93 | 43.38 | 39.69 | 4.015 |
| 2.177 | 92.50 | 42.49 | 39.30 | 4.739 |
| 2.303 | 98.69 | 42.85 | 39.64 | 5.304 |
| 2.455 | 104.76 | 42.67 | 39.66 | 6.028 |
| 2.594 | 111.48 | 42.97 | 40.12 | 6.729 |
| 2.718 | 117.83 | 43.35 | 40.63 | 7.389 |
| 2.843 | 122.76 | 43.18 | 40.58 | 8.084 |
| 2.965 | 127.18 | 42.90 | 40.41 | 8.789 |
| 3.089 | 135.07 | 43.73 | 41.34 | 9.541 |
| 3.212 | 138.28 | 43.05 | 40.75 | 10.319 |
| 3.367 | 146.02 | 43.37 | 41.18 | 11.338 |
| 3.509 | 154.85 | 44.13 | 42.02 | 12.312 |
| 3.602 | 158.92 | 44.12 | 42.07 | 12.974 |
| 3.627 | 159.24 | 43.89 | 41.87 | 13.159 |
| 3.878 | 171.74 | 44.28 | 42.38 | 15.041 |
| 4.039 | 180.98 | 44.81 | 42.98 | 16.313 |
| 4.235 | 190.59 | 45.01 | 43.27 | 17.933 |
| 4.453 | 199.61 | 44.82 | 43.16 | 19.831 |
| 4.682 | 211.96 | 45.27 | 43.69 | 21.917 |
| 4.944 | 227.77 | 45.07 | 44.58 | 24.441 |

**Table 11: Specific Heat Data for $Cr_{72.75} Fe_{24.25} Si_{3.00}$**

| $T$ $(^\circ K)$ | $C$ (In $10^{-4}$ Cal. mol.$^{-1}$ deg.$^{-1}$) | $C/T$ (In $10^{-4}$ Cal. mol.$^{-1}$ deg.$^{-2}$) | $(C-A)/T$ (In $10^{-4}$ Cal. mol.$^{-1}$ deg.$^{-2}$) | $T^2$ $(^\circ K^2)$ |
|---|---|---|---|---|
| 1.321 | 42.68 | 32.31 | 24.17 | 1.745 |
| 1.367 | 44.32 | 32.42 | 24.56 | 1.869 |
| 1.410 | 44.84 | 31.80 | 24.18 | 1.988 |
| 1.451 | 46.16 | 31.81 | 24.41 | 2.105 |
| 1.551 | 48.19 | 31.07 | 24.15 | 2.405 |
| 1.629 | 50.60 | 31.06 | 24.47 | 2.654 |
| 1.650 | 50.95 | 30.88 | 24.37 | 2.723 |
| 1.720 | 53.46 | 31.08 | 24.84 | 2.958 |
| 1.724 | 53.24 | 30.88 | 24.65 | 2.972 |
| 1.825 | 54.73 | 29.99 | 24.10 | 3.331 |
| 1.942 | 58.34 | 30.04 | 24.51 | 3.771 |
| 2.047 | 61.51 | 30.05 | 24.80 | 4.190 |
| 2.187 | 65.61 | 30.00 | 25.09 | 4.783 |
| 2.370 | 70.72 | 29.84 | 25.31 | 5.617 |
| 2.539 | 76.40 | 30.09 | 25.86 | 6.446 |
| 2.690 | 78.71 | 29.26 | 25.27 | 7.236 |
| 2.871 | 85.13 | 29.65 | 25.91 | 8.243 |
| 3.106 | 91.88 | 29.58 | 26.12 | 9.647 |
| 3.420 | 104.31 | 30.50 | 27.36 | 11.696 |
| 3.630 | 110.32 | 30.39 | 27.43 | 13.177 |
| 3.857 | 116.91 | 30.31 | 27.53 | 14.876 |
| 4.099 | 128.18 | 31.27 | 28.65 | 16.802 |
| 4.384 | 138.23 | 31.53 | 29.08 | 19.219 |
| 4.642 | 147.71 | 31.82 | 29.51 | 21.548 |

Table 12: Specific Heat Data for $Cr_{67.90} Fe_{29.10} Si_{3.00}$

| $T$ ($^{\circ}K$) | $C$ (In $10^{-4}$ Cal. mol.$^{-1}$ deg.$^{-1}$) | $C/T$ (In $10^{-4}$ Cal. mol.$^{-1}$ deg.$^{-2}$) | $(C-A)/T$ (In $10^{-4}$ Cal. mol.$^{-1}$ deg.$^{-2}$) | $T^2$ ($^{\circ}K^2$) |
|---|---|---|---|---|
| 1.348 | 35.35 | 26.22 | 16.91 | 1.915 |
| 1.447 | 37.07 | 25.62 | 16.95 | 2.094 |
| 1.502 | 38.07 | 25.34 | 16.98 | 2.256 |
| 1.663 | 42.70 | 25.68 | 18.13 | 2.766 |
| 1.762 | 42.84 | 24.32 | 17.19 | 3.104 |
| 2.015 | 48.18 | 23.91 | 17.68 | 4.060 |
| 2.232 | 52.31 | 23.43 | 17.81 | 4.982 |
| 2.444 | 55.49 | 22.71 | 17.57 | 5.973 |
| 2.620 | 61.55 | 23.49 | 18.70 | 6.864 |
| 2.804 | 67.55 | 24.09 | 19.61 | 7.862 |
| 2.999 | 72.24 | 24.09 | 20.07 | 8.994 |
| 3.314 | 80.62 | 24.33 | 20.54 | 10.982 |
| 3.707 | 90.20 | 24.33 | 20.95 | 13.742 |
| 4.017 | 101.30 | 25.22 | 22.09 | 16.136 |
| 4.278 | 112.09 | 26.20 | 23.27 | 18.301 |
| 4.537 | 120.45 | 26.55 | 23.78 | 20.584 |

## Table 13: Specific Heat Data for $Cr_{48.5}$ $Fe_{48.5}$ $Si_{3.00}$

| T ($^\circ$K) | C (In $10^{-4}$ Cal. mol.$^{-1}$ deg.$^{-1}$) | C/T (In $10^{-4}$ Cal. mol.$^{-1}$ deg.$^{-2}$) | $T^2$ ($^\circ$K$^2$) |
|---|---|---|---|
| 1.202 | 17.12 | 14.25 | 1.444 |
| 1.220 | 17.31 | 14.18 | 1.489 |
| 1.241 | 17.68 | 14.24 | 1.540 |
| 1.258 | 17.90 | 14.23 | 1.582 |
| 1.282 | 18.18 | 14.18 | 1.644 |
| 1.298 | 18.24 | 14.05 | 1.684 |
| 1.322 | 18.93 | 14.32 | 1.747 |
| 1.351 | 19.48 | 14.42 | 1.826 |
| 1.411 | 20.19 | 14.31 | 1.991 |
| 1.424 | 20.17 | 14.16 | 2.029 |
| 1.486 | 20.97 | 14.11 | 2.209 |
| 1.502 | 21.38 | 14.23 | 2.255 |
| 1.534 | 21.55 | 14.04 | 2.354 |
| 1.541 | 21.81 | 14.15 | 2.374 |
| 1.576 | 22.12 | 14.04 | 2.484 |
| 1.629 | 22.93 | 14.07 | 2.654 |
| 1.687 | 23.79 | 14.09 | 2.848 |
| 1.742 | 24.21 | 13.89 | 3.034 |
| 1.827 | 26.09 | 14.28 | 3.337 |
| 1.871 | 26.79 | 14.31 | 3.501 |
| 1.950 | 27.68 | 14.19 | 3.802 |
| 1.996 | 28.50 | 14.28 | 3.984 |
| 2.119 | 30.25 | 14.27 | 4.492 |
| 2.162 | 30.50 | 14.11 | 4.673 |
| 2.227 | 31.34 | 14.07 | 4.958 |
| 2.274 | 32.16 | 14.15 | 5.169 |
| 2.411 | 34.66 | 14.37 | 5.813 |
| 2.450 | 35.35 | 14.43 | 6.003 |
| 2.601 | 37.80 | 14.53 | 6.766 |
| 2.681 | 38.72 | 14.44 | 7.190 |
| 2.701 | 39.15 | 14.51 | 7.296 |
| 2.855 | 41.44 | 14.52 | 8.150 |
| 2.873 | 42.02 | 14.63 | 8.253 |
| 3.033 | 44.46 | 14.66 | 9.200 |
| 3.049 | 44.50 | 14.60 | 9.294 |
| 3.248 | 48.04 | 14.79 | 10.548 |
| 3.252 | 47.82 | 14.70 | 10.576 |
| 3.287 | 48.51 | 14.76 | 10.807 |
| 3.461 | 51.72 | 14.95 | 11.976 |
| 3.464 | 52.08 | 15.04 | 11.998 |
| 3.640 | 55.48 | 15.24 | 13.252 |
| 3.809 | 58.83 | 15.45 | 14.505 |
| 3.955 | 60.97 | 15.41 | 15.645 |
| 4.023 | 62.88 | 15.63 | 16.181 |
| 4.257 | 66.34 | 15.58 | 18.123 |
| 4.291 | 68.36 | 15.93 | 18.412 |
| 4.549 | 73.95 | 16.25 | 20.699 |
| 4.787 | 78.75 | 16.45 | 22.913 |

Table 14: Specific Heat Data for $Cr_{24.25} Fe_{72.75} Si_{3.00}$

| $T$ ($^\circ$K) | $C$ (In $10^{-4}$ Cal. mol.$^{-1}$ deg.$^{-1}$) | $C/T$ (In $10^{-4}$ Cal. mol.$^{-1}$ deg.$^{-2}$) | $T^2$ ($^\circ$K$^2$) |
|---|---|---|---|
| 1.266 | 13.54 | 10.70 | 1.603 |
| 1.342 | 14.26 | 10.63 | 1.801 |
| 1.397 | 14.76 | 10.56 | 1.952 |
| 1.448 | 15.26 | 10.53 | 2.098 |
| 1.457 | 15.46 | 10.61 | 2.124 |
| 1.519 | 16.03 | 10.55 | 2.308 |
| 1.569 | 16.13 | 10.28 | 2.462 |
| 1.579 | 16.81 | 10.65 | 2.493 |
| 1.640 | 16.94 | 10.33 | 2.690 |
| 1.729 | 18.07 | 10.45 | 2.889 |
| 1.736 | 18.00 | 10.37 | 3.015 |
| 1.800 | 18.63 | 10.35 | 3.241 |
| 1.839 | 19.69 | 10.71 | 3.382 |
| 1.866 | 19.28 | 10.33 | 3.483 |
| 1.938 | 20.17 | 10.41 | 3.758 |
| 2.014 | 21.19 | 10.52 | 4.058 |
| 2.091 | 21.91 | 10.48 | 4.372 |
| 2.197 | 23.13 | 10.53 | 4.826 |
| 2.331 | 24.85 | 10.66 | 5.436 |
| 2.432 | 24.63 | 10.52 | 5.484 |
| 2.473 | 26.36 | 10.66 | 6.114 |
| 2.476 | 26.33 | 10.64 | 6.129 |
| 2.619 | 27.46 | 10.48 | 6.862 |
| 2.634 | 28.09 | 10.66 | 6.941 |
| 2.800 | 29.92 | 10.68 | 7.841 |
| 2.995 | 32.34 | 10.78 | 8.968 |
| 3.203 | 34.84 | 10.88 | 10.263 |
| 3.239 | 35.33 | 10.90 | 10.493 |
| 3.458 | 37.90 | 10.95 | 11.960 |
| 3.647 | 40.27 | 11.04 | 13.302 |
| 3.872 | 43.92 | 11.34 | 14.995 |
| 4.076 | 47.03 | 11.54 | 16.613 |
| 4.289 | 50.20 | 11.70 | 18.395 |
| 4.491 | 52.31 | 11.65 | 20.168 |
| 4.722 | 55.85 | 11.83 | 22.293 |

Table 15:  Specific  Heat Data for $Cr_{4.85}$ $Fe_{92.15}$ $Si_{3.00}$

| T ($^\circ$K) | C (In $10^{-4}$ Cal. mol.$^{-1}$ deg.$^{-1}$) | C/T (In $10^{-4}$ Cal. mol.$^{-1}$ deg.$^{-2}$) | $T^2$ ($^\circ$K$^2$) |
|---|---|---|---|
| 1.307 | 14.20 | 10.86 | 1.708 |
| 1.385 | 15.06 | 10.87 | 1.919 |
| 1.439 | 15.44 | 10.73 | 2.070 |
| 1.461 | 15.98 | 10.94 | 2.134 |
| 1.515 | 16.09 | 10.62 | 2.295 |
| 1.629 | 17.36 | 10.66 | 2.652 |
| 1.674 | 17.99 | 10.75 | 2.801 |
| 1.775 | 19.32 | 10.88 | 3.151 |
| 1.846 | 19.80 | 10.72 | 3.409 |
| 1.859 | 19.97 | 10.74 | 3.457 |
| 1.953 | 20.74 | 10.62 | 3.816 |
| 2.017 | 21.32 | 10.57 | 4.067 |
| 2.080 | 22.42 | 10.78 | 4.327 |
| 2.131 | 23.25 | 10.91 | 4.542 |
| 2.233 | 24.26 | 10.86 | 4.987 |
| 2.382 | 26.26 | 11.03 | 5.674 |
| 2.546 | 28.34 | 11.13 | 6.481 |
| 2.789 | 30.88 | 11.07 | 7.778 |
| 2.891 | 32.19 | 11.14 | 8.358 |
| 3.099 | 35.29 | 11.39 | 9.599 |
| 3.132 | 35.59 | 11.36 | 9.808 |
| 3.204 | 36.07 | 11.26 | 10.264 |
| 3.356 | 39.67 | 11.82 | 11.260 |
| 3.505 | 40.45 | 11.54 | 12.287 |
| 3.588 | 41.71 | 11.62 | 12.876 |
| 3.718 | 43.71 | 11.76 | 13.826 |
| 3.809 | 44.87 | 11.78 | 14.513 |
| 3.928 | 46.50 | 11.84 | 15.426 |
| 4.123 | 48.82 | 11.84 | 17.003 |
| 4.300 | 51.79 | 12.04 | 18.984 |
| 4.539 | 56.44 | 12.43 | 20.604 |
| 4.879 | 63.21 | 12.96 | 23.807 |

Table 16:  Low temperature specific heat of $(Cr_xFe_{1-x})_{97}Si_3$ Alloys using two parameter and three parameter equations [Eqns.(1.1) and (4.3)].

| Alloys | $A \times 10^4$ (Cal.mol.$^{-1}$ deg.$^{-1}$) | $\gamma \times 10^4$ (Cal.mol.$^{-1}$ deg.$^{-2}$) | $\beta \times 10^4$ (Cal.mol.$^{-1}$ deg.$^{-4}$) | $\theta_D$ (°K) | RMS Deviations of Cx10$^4$ (Cal.mol.$^{-1}$ deg.$^{-1}$) |
|---|---|---|---|---|---|
| $Cr_{97}Si_3$ | — | 6.14 | 0.0527 | 445 | 0.16 |
| $Cr_{97}Si_3$ | 8.82 | 19.63 | -0.0288 | — | 0.54 |
| $(Cr_{95}Fe_5)_{97}Si_3$ $(Cr_{92.15}Fe_{4.85}Si_{3.00})$ | — | 21.21* | 0.0132* | 706* | — |
| $(Cr_{90}Fe_{10})_{97}Si_3$ $(Cr_{87.30}Fe_{9.70}Si_{3.00})$ | — | 44.20 | 0.0155 | 669 | 0.54 |
| $(Cr_{85}Fe_{15})_{97}Si_3$ $(Cr_{82.45}Fe_{14.55}Si_{3.00})$ | 14.61 | 41.84 | 0.1354 | 325 | 0.85 |
| $(Cr_{80}Fe_{20})_{97}Si_3$ $(Cr_{77.60}Fe_{19.40}Si_{3.00})$ | 7.39 | 38.59 | 0.2439 | 267 | 1.01 |
| $(Cr_{75}Fe_{25})_{97}Si_3$ $(Cr_{72.75}Fe_{24.25}Si_{3.00})$ | 10.74 | 23.67 | 0.2790 | 255 | 0.72 |
| $(Cr_{70}Fe_{30})_{97}Si_3$ $(Cr_{67.90}Fe_{29.10}Si_{3.00})$ | 12.55 | 16.25 | 0.3688 | 242 | 1.06 |
| $(Cr_{50}Fe_{50})_{97}Si_3$ $(Cr_{48.50}Fe_{48.50}Si_{3.00})$ | — | 13.74 | 0.1130 | 345 | 0.42 |
| $(Cr_{25}Fe_{75})_{97}Si_3$ $(Cr_{24.50}Fe_{72.50}Si_{3.00})$ | — | 10.19 | 0.0742 | 397 | 0.30 |
| $(Cr_5Fe_{95})_{97}Si_3$ $(Cr_{4.85}Fe_{92.15}Si_{3.00})$ | — | 10.39 | 0.0983 | 362 | 0.41 |

\* Extrapolated

SAMPLE: $Cr_{24.25} Fe_{72.75} Si_{3.00}$
MEASURING CURRENT: 1.0 $\mu$ A
HEATING CURRENT: 0.2 m A
BALANCING EMF 5000 $\mu$ V BEFORE HEAT PULSE,
4000 $\mu$ V AFTER HEAT PULSE.
AMPLIFIER SCALE: 1000 X.
HEATING PERIOD: 44.24 SECS.

142 $\mu$ V

300 $\mu$ V
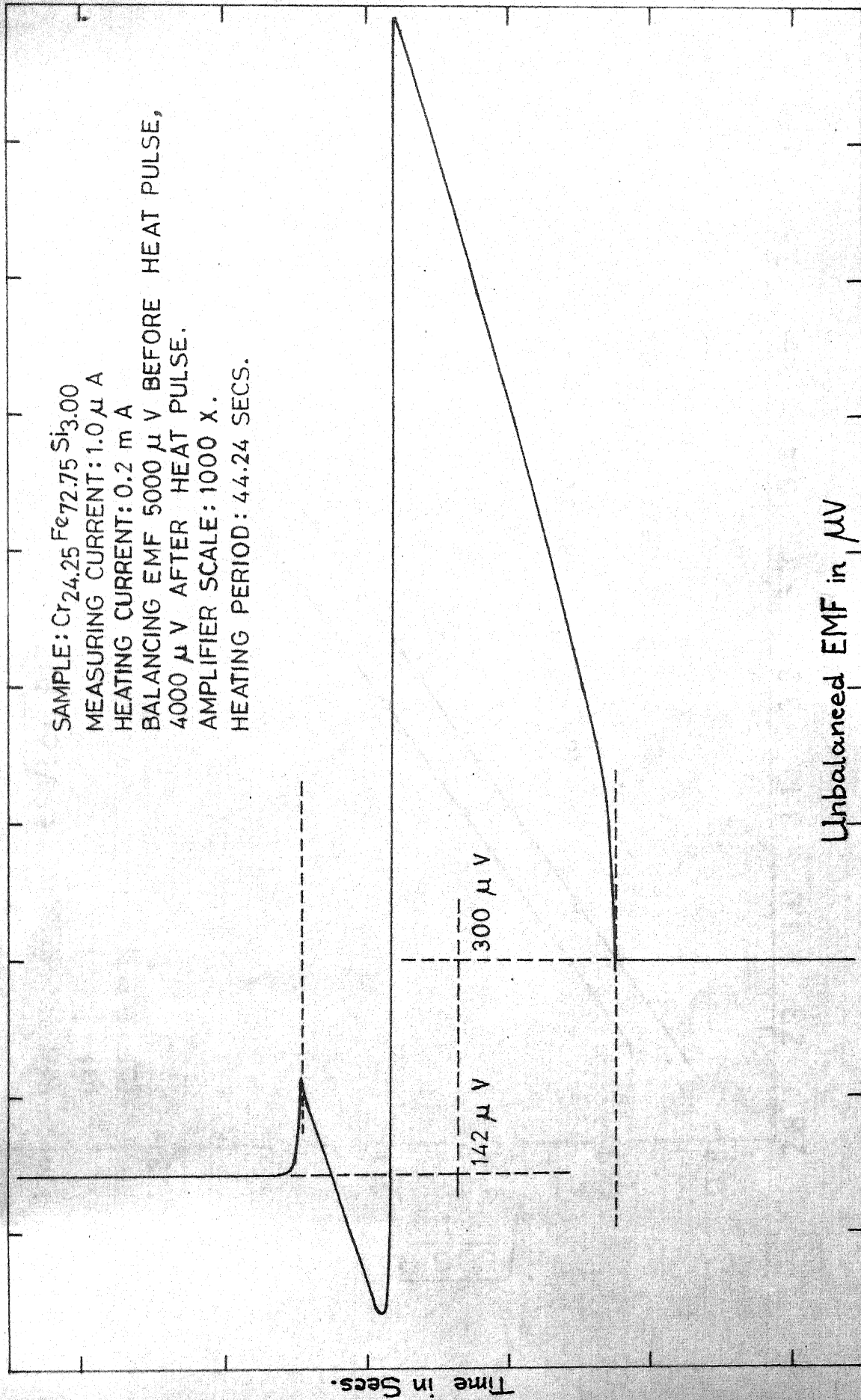
Time in Secs.

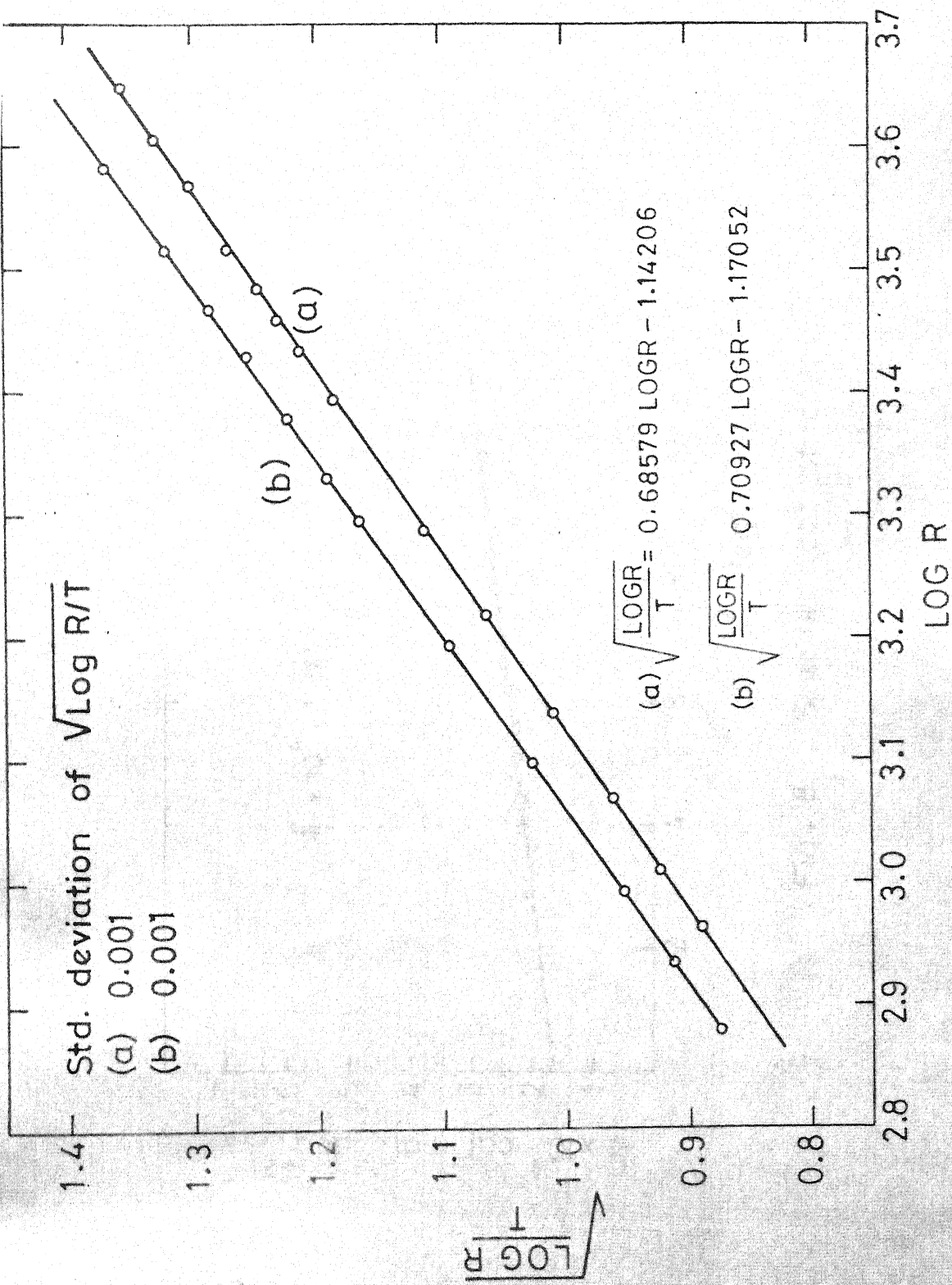Unbalanced EMF in $\mu$ V

Fig.,6  A typical heating curve

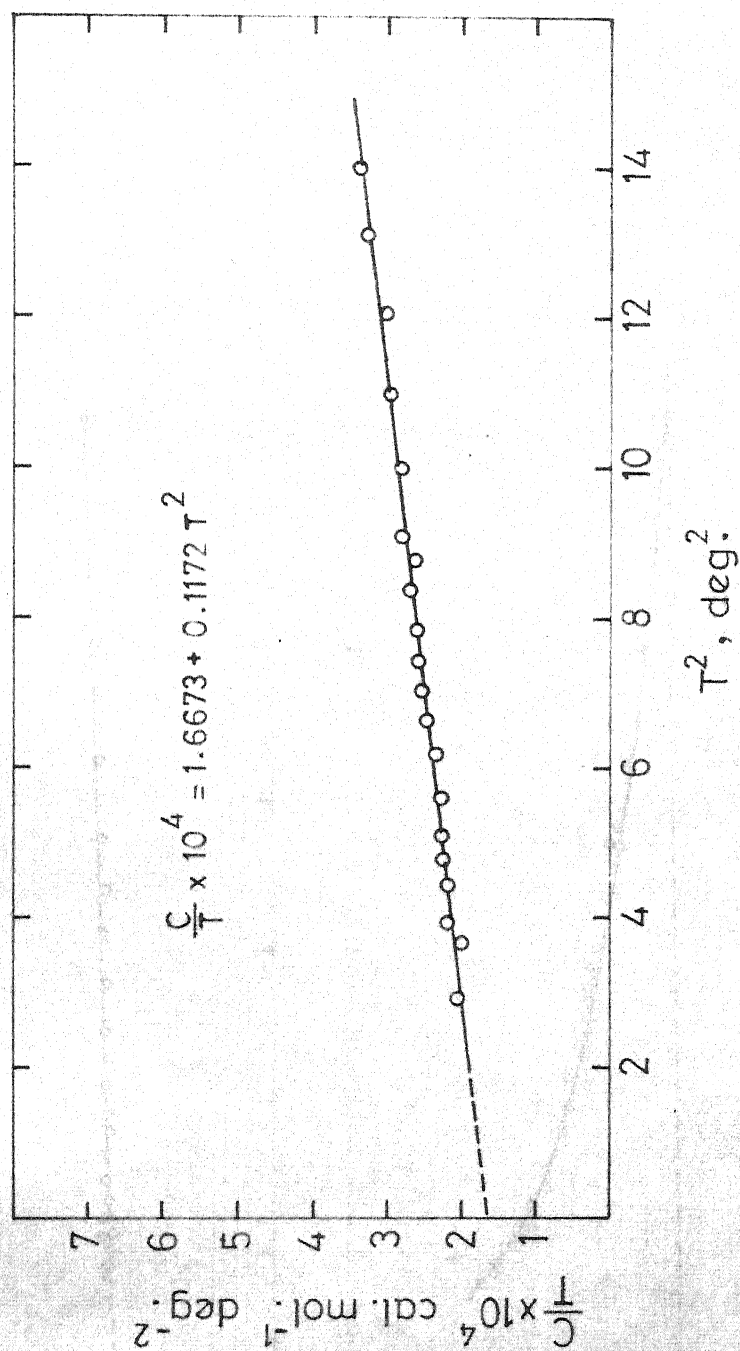Fig. 7   Calibration curves for two carbon thermometers.
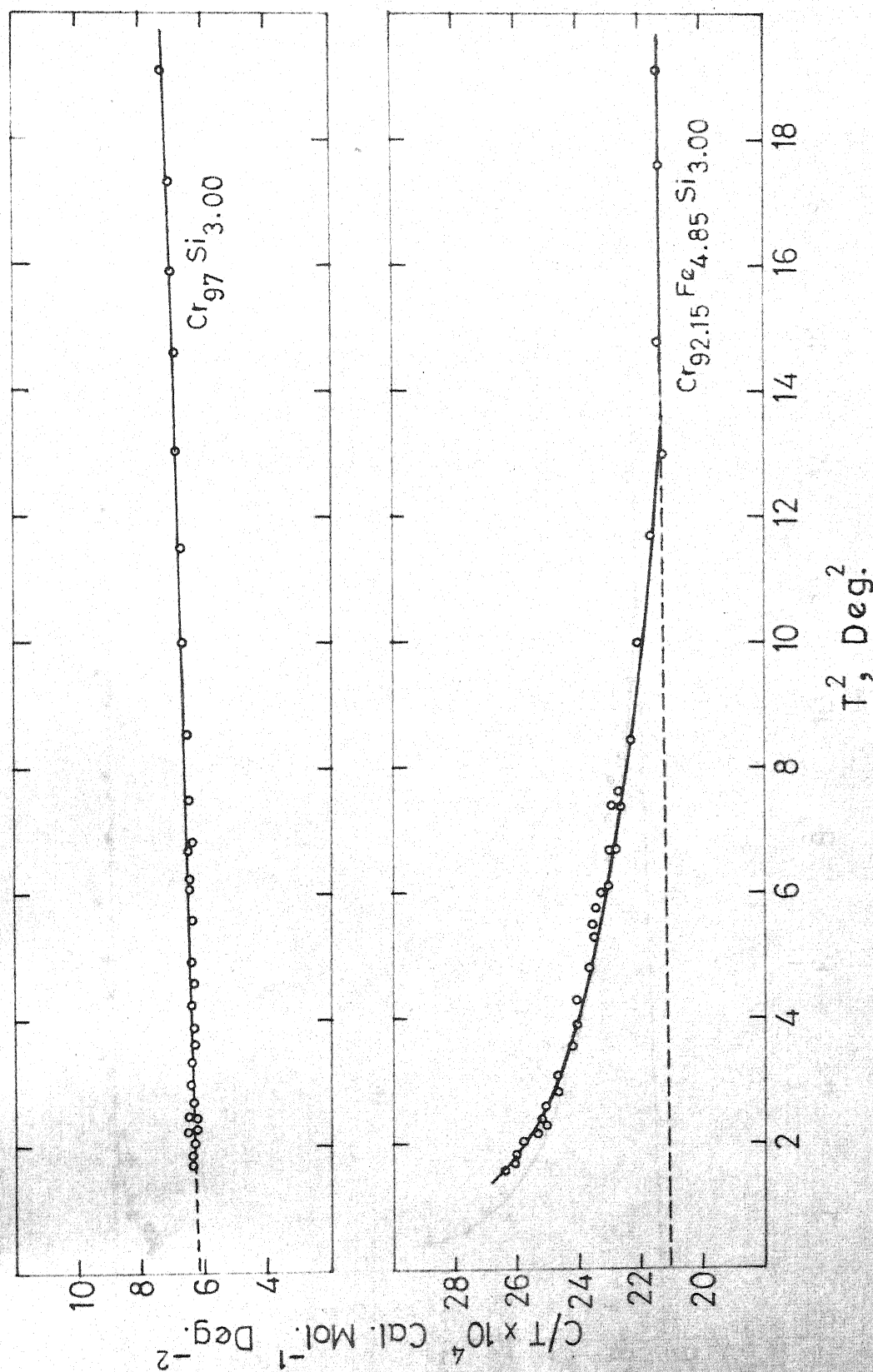
Fig. 8   Specific heat of copper

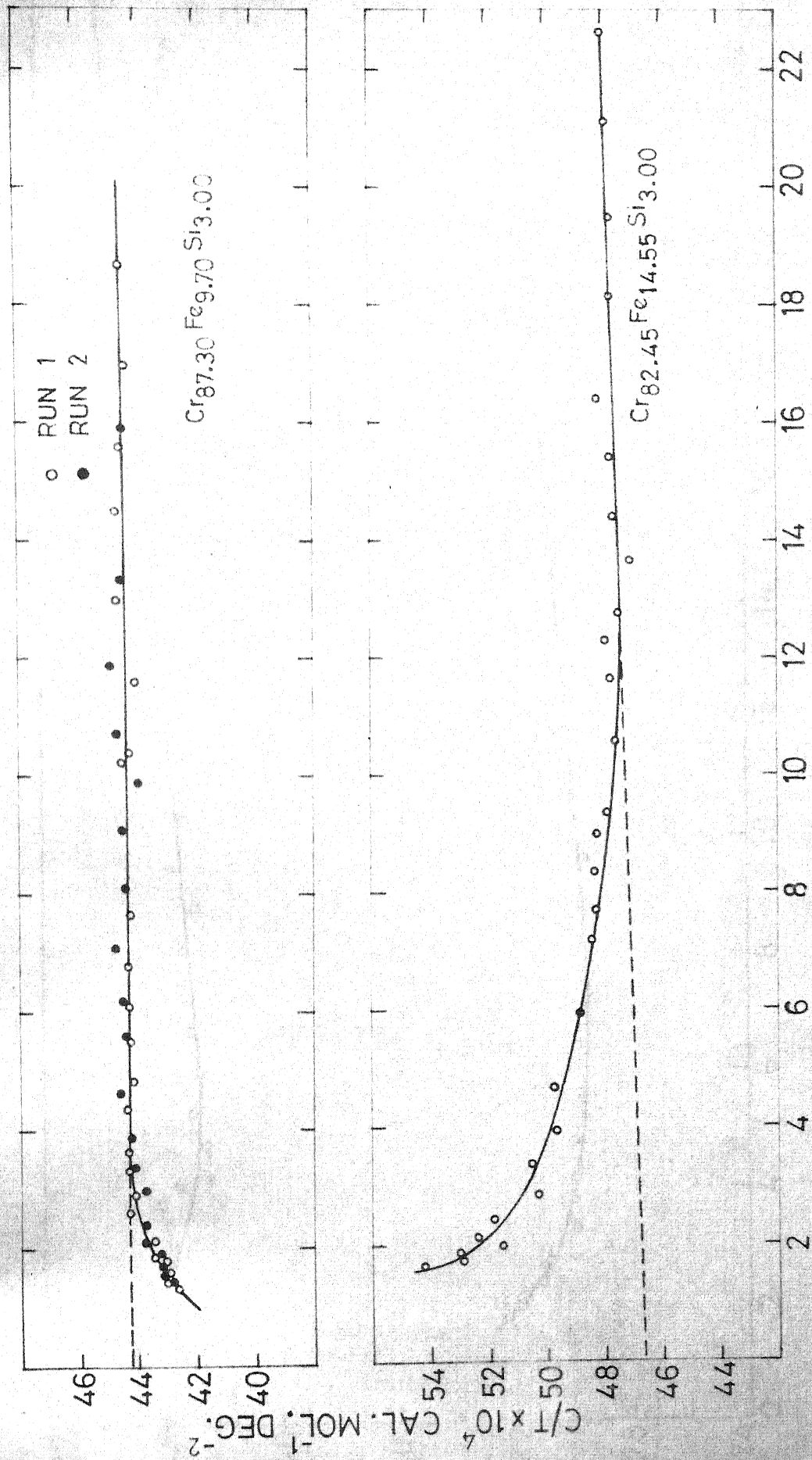Fig. 9 Specific heat of Cr-Si and Cr-Fe-Si alloys

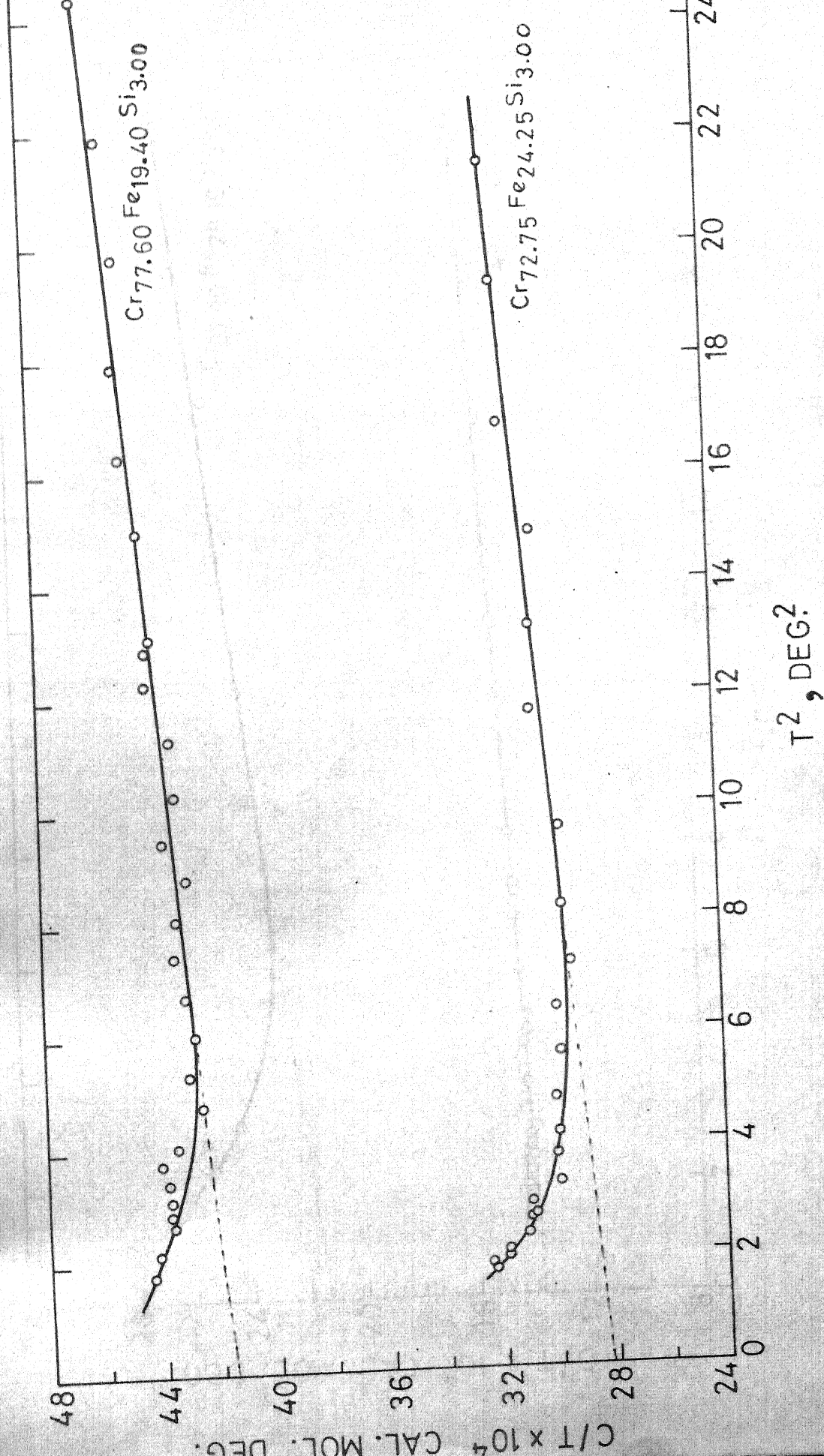FIG.10 Specific heat of Cr-Fe-Si alloys
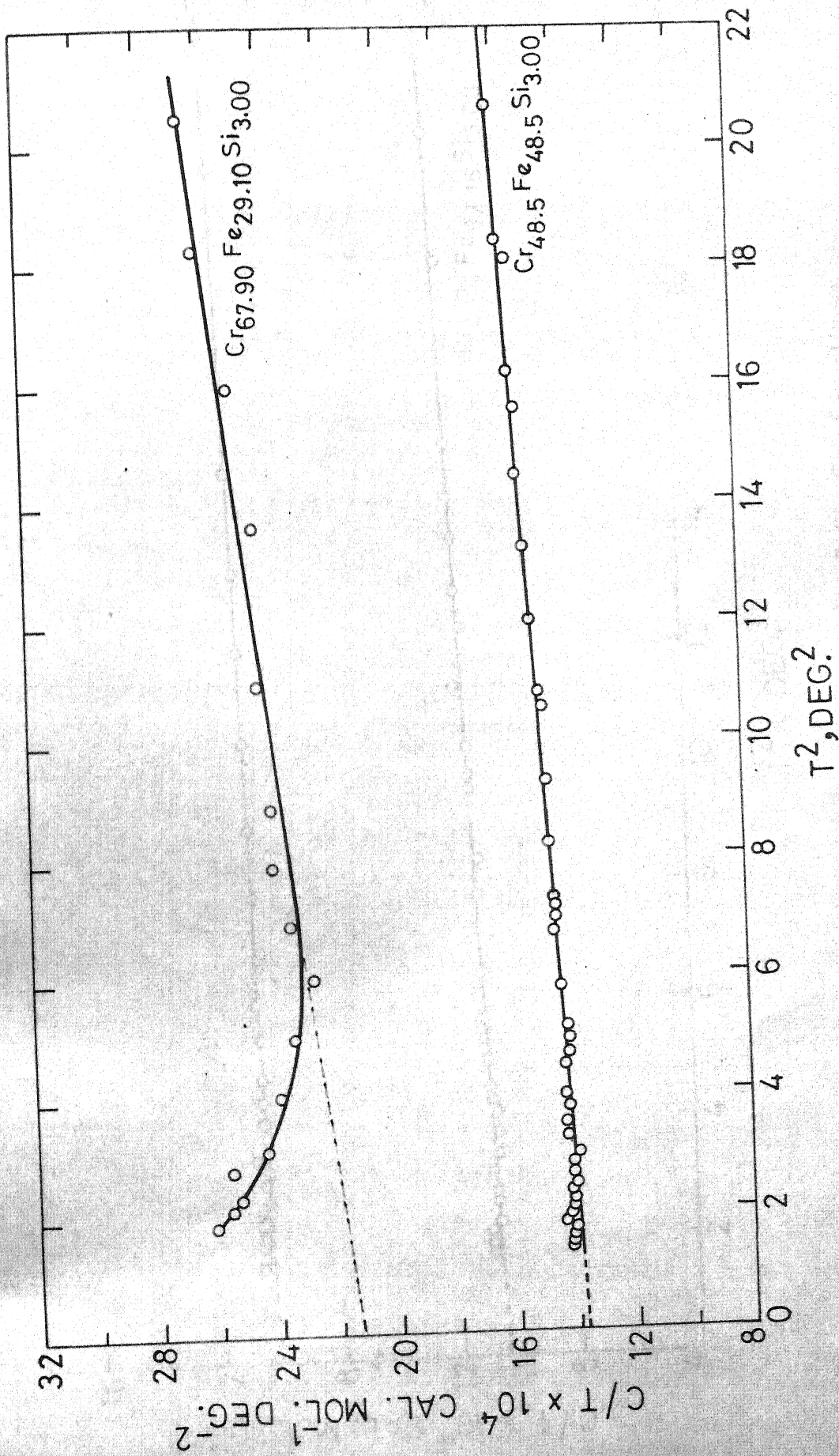
Fig. 11    Specific heat of Cr–Fe–Si alloys
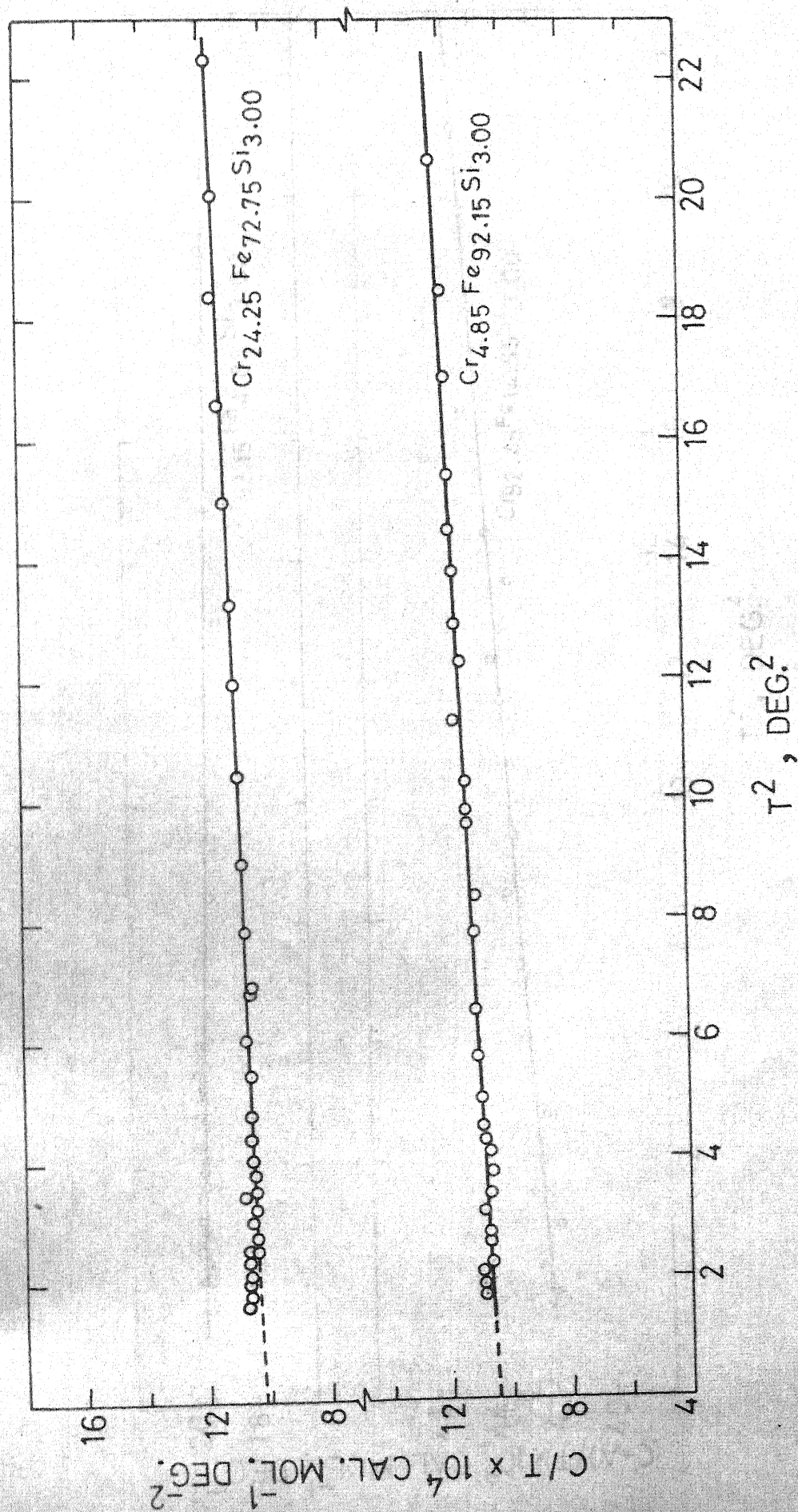
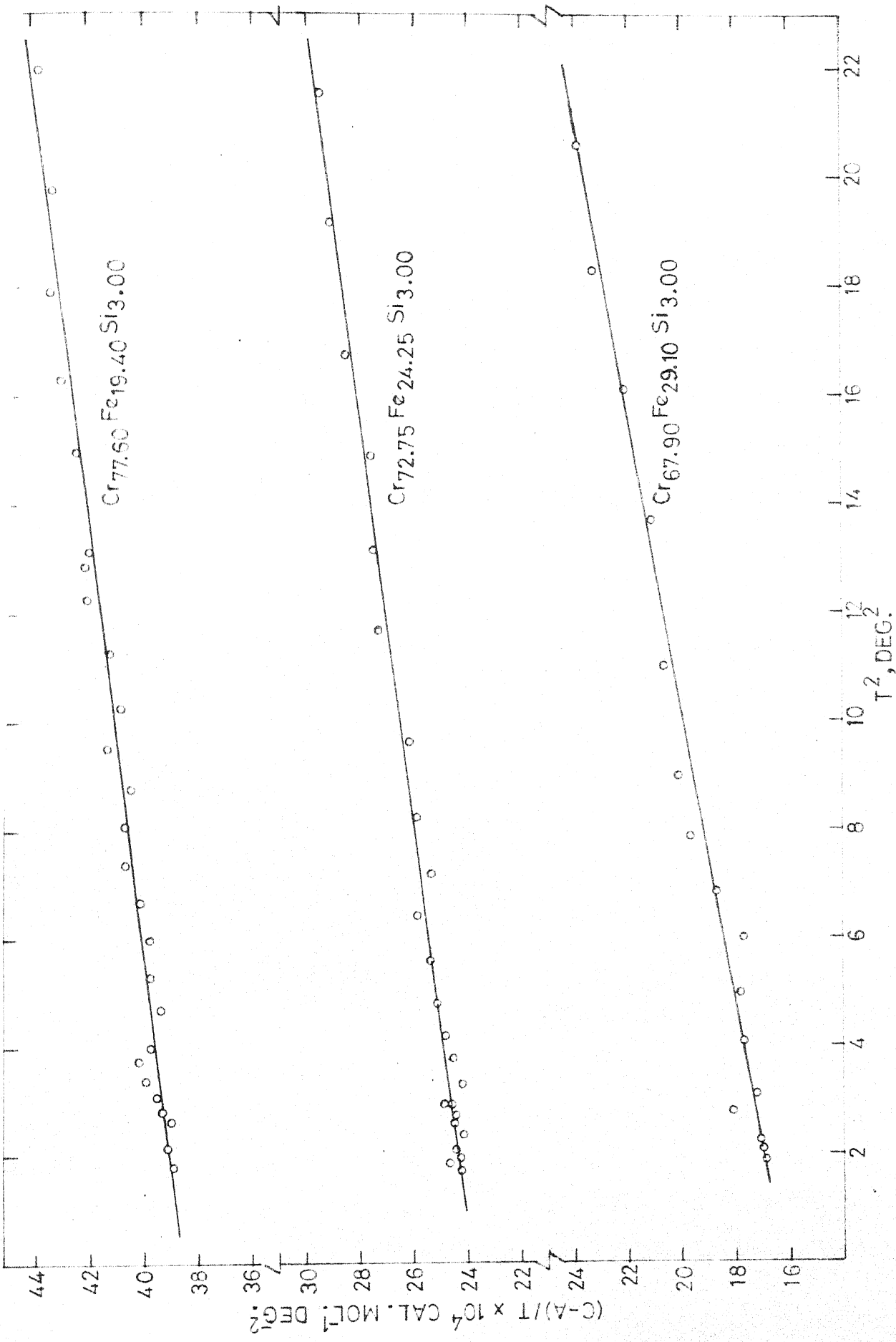Fig. 12    Specific heat of Cr-Fe-Si alloys

Fig. 13    Specific heat of Cr-Fe-Si alloys

Fig.15 (C-A)/T vs. T² plot of Cr-Fe-Si alloys

# CHAPTER V

## DISCUSSION

The specific heat data of the series of alloys $(Cr_xFe_{1-x})_{97}Si_3$ investigated are shown in Figures 9-15 and listed in Tables 6-16. From the data it is clear that the specific heat data for the entire range of the binary $Cr_{97}Si_3$ and the ternary $(Cr_xFe_{1-x})_{97}Si_3$ alloys investigated may be divided into three groups characterised by their response to the two term specific heat relation $C = \gamma T + \beta T^3$ (equation 1.1). These are,

(i) the alloys showing straightline relationship in their $C/T$ vs. $T^2$ plots,

(ii) the alloys showing 'upturn' effect when $C/T$ is plotted as a function of $T^2$,

(iii) the third group consisting of a solitary example, $(Cr_{90}Fe_{10})_{97}Si_3$, in which the $C/T$ vs. $T^2$ is a straight line down to about $1.5^\circ K$, and below which the curve droops downwards.

The binary $Cr_{97}Si_3$ and the ternary $(Cr_{50}Fe_{50})_{97}Si_3$, $(Cr_{25}Fe_{75})_{97}Si_3$ and $(Cr_5Fe_{95})_{97}Si_3$ alloys constitute the first group. From the $C/T$ vs. $T^2$ plots of these alloys shown in Figures 9,12 and 13, it is clear that they give well defined straight lines, from which $\gamma$ and $\beta$ values could be obtained directly by the least squares method. From the magnetic data of $(Cr_xFe_{1-x})$ alloys[48,49] and in view of the limited dilution

by Si it is expected that the ternary alloys belonging to this group should be ferromagnetic. A simple test involving attraction of the specimens by a small permanent magnet confirmed that these ternary alloys are distinctly ferromagnetic with their Curie temperatures above the ambient temperature, $25°C$. The distinctly ferromagnetic alloys in the ternary systems $(Cr_xFe_{1-x})_{90}Al_{10}$[34] and $(Cr_xFe_{1-x})_{80}Al_{20}$[37] and in the binary system $(Cr_xFe_{1-x})$[21] show similar normal straight line $C/T$ vs. $T^2$ plots. Cr metal is antiferromagnetic below $310°K$, but there is no published data on the magnetic structure of Cr-Si alloys. However, the binary alloys of Cr with the several transition metals show[50,51] that the antiferromagnetism is retained (though the spin density wave vector changes) upto a considerable concentration of the transition metal solute. Similarly, published data on Cr-Al alloys[38] show that upto about 30 at% Al the alloys are antiferromagnetic. Thus, even in the absence of actual data on Cr-Si alloys it is reasonable to assume that the $Cr_{97}Si_3$ binary alloy is antiferromagnetic. The specific heat data for the $Cr_{97}Si_3$ alloy (Figure 9) like the antiferromagnetic Cr-Al alloys[34] show a normal straight line behaviour in the $C/T$ vs. $T^2$ plot. Thus the behaviour of the $Cr_{97}Si_3$ and the ferromagnetic Cr-Fe-Si alloys are in accordance with the observations[20] that metals and alloys in their normal non-super conducting states and with simple spin structure generally show straight line relationship in $C/T$ vs. $T^2$ plot.

The Debye temperature $\theta_D$ for the antiferromagnetic pure Cr reported in the literature[20] varies over a rather wide range from $400^\circ$K to $630^\circ$K. No clear picture is available for such wide variation in the experimental value of $\theta_D$. This has often been attributed[20] to the presence of small amounts of other elements present in solid solutions, or in a yet unknown way on the state of the sample in terms of internal strains, dislocation density and such other effects. However, $\theta_D \approx 600^\circ$K seems to be the reasonable value for $Cr$[20]. The $\theta_D$ value calculated for the present $Cr_{97}Si_3$ alloy is $445^\circ$K, indicating that a small amount of Si dissolved in Cr is apparently increasing the $\beta$ value and therefore, the lattice contribution to the total specific heat. This effect of an alloying element on the Debye temperature was also observed in Cr-Al alloy system[34] in which a decrease of $\theta_D$ to about $440^\circ$K was achieved by about 25 at% Al. This together with the $\theta_D$ values of high Fe alloys in the Cr-Fe-Al systems[34,37] indicate that Si affects the lattice contribution to specific heat more than Al. The $\theta_D$ values of the alloys $(Cr_{50}Fe_{50})_{97}Si_3$ and $(Cr_{25}Fe_{75})_{97}Si_3$, $345^\circ$K and $397^\circ$K, respectively are comparable to those of the binary alloys of $(Cr_x Fe_{1-x})$ system[21] but the $\theta_D$ value of $348^\circ$k for the $(Cr_5Fe_{95})_{97}Si_3$ alloy is much smaller than that of the closely analogous binary alloy $(Cr_6Fe_{94})$ for which it is $475^\circ$K [21]. It is difficult at this stage to resolve such large difference of $\theta_D$ values between these two closely analogous alloys where the third alloying element content is rather small.

The second group of alloys are those with Cr:Fe ratio greater than 50:50. These alloys are, $(Cr_{95}Fe_5)_{97}Si_3$, $(Cr_{85}Fe_{15})_{97}Si_3$, $(Cr_{80}Fe_{20})_{97}Si_3$, $(Cr_{75}Fe_{25})_{97}Si_3$ and $(Cr_{70}Fe_{30})_{97}Si_3$. The C/T vs. $T^2$ plots for these alloys show 'upturn' anomaly. Similar anomaly has been observed in several binary $(Cr_xFe_{1-x})$[21], ternary $(Cr_xFe_{1-x})_{90}Al_{10}$[34] and $(Cr_xFe_{1-x})_{80}Al_{20}$[37] alloys. The upturn anomaly in alloys which have no hyperfine interactions and are not superconducting is generally attributed to either of the two reasons: (i) many-body effects[52-54], and (ii) super paramagnetic cluster effects[47,55-56]. The many body effects responsible for the enhancement of low temperature specific heat in the alloys close to the critical composition for ferromagnetism is concerned with the interaction between the spin density fluctuations (paramagnons) and the d electrons of the alloys of the transition metals. In this approach the specific heat is enhanced by a factor,

$$A(T) \approx (T/T_s)^3 \ln (T/T_s) \tag{5.1}$$

where $T_s = T_F(1-\bar{I})$, with $T_F$ the degeneracy temperature and $\bar{I} = IN(E_f)$ involving the effective interaction energy between the d electrons in the alloys of the transition metals and the paramagnons, and the single particle density of states at the Fermi level.

It has however been shown[53] that the form $A(T) \approx (T/T_s)^3 \ln (T/$ of the anomaly may only be applicable at exceedingly low temperatures

The $(C-A)/T$ vs. $T^2$ plots for the present alloys are shown in Figures 14 and 15. Reasonably good fit of the data with a straight line could be obtained, as is evident from the standard deviations (Table 16), when the cluster specific heat was considered. The specific heat data for the analogous alloys in the system $(Cr_xFe_{1-x})_{90}Al_{10}$[34] could be analysed in terms of the three parameter equation $C = A + \gamma T + \beta T^3$. However, for the system $(Cr_xFe_{1-x})_{80}Al_{20}$ Srinivasan et al.[37] found it necessary to use the complete Einstein function in place of the constant A in the three parameter equation (4.3). Therefore, it may be concluded that the super paramagnetic particle model appears to explain reasonably well the low temperature anomaly in the specific heat data of the Cr-Fe-Si alloys.

The upturn effect of Cr-Fe-Si alloys upto 29.1 at% Fe alloy (Cr: Fe = 70:30), except for the 9.70 at% Fe alloy (Cr:Fe = 90:10) is similar in nature as that observed in Cr-Fe-Al alloys;[34,37] throughout the whole range of composition upturn effect is observed till the material became distinctly ferromagnetic. This is contrary to that observed[21] for the binary Cr-Fe alloys in which upturn effect was observed for very low Fe containing alloys and then only for the alloy for which the maximum $\gamma$ value was obtained. The Cr-Fe-Al alloys showed that the maximum upturn, as indicated by the value of A, determined by the unrestricted solution of the specific heat equations, was at higher Fe: Cr ratio as the Al content was increased. The Cr-Fe-Si alloys also show that the addition of Si produces the largest upturn in the same composition

region as that of the $(Cr_xFe_{1-x})_{90}Al_{10}$ alloys, namely at $(Cr_{85}Fe_{15})_{97}Si_3$, and not at the Cr:Fe ratio of 95:5 as in the binary Cr-Fe alloys. Since the upturn effect is due to the enhancement of the specific heat C by the term A which is related to the number of clusters per mole (equation 5.3), the shift of the maximum upturn to higher Fe:Cr ratio with the addition of Si and Al would indicate that the value of N is dependent on the nature and the amount of the third element in the Cr-Fe-X alloys, where X is a non-transition element, Al or Si.

In an attempt to correlate the magnetic state and the presence of upturn anomaly in the present alloys, a simple test involving attraction of the specimen, cooled down to liquid $N_2$ temperature, by a small permanent magnet was performed. The test indicated that the alloys upto 14.55 at% Fe are not attracted by the magnet even at $77^O$K and hence can be said to be non magnetic. The 19.40 at% Fe alloy was feebly attracted by the magnet at $77^O$K and is barely ferromagnetic, and all the other alloys are ferromagnetic. The upturn effect in the present Cr-Fe-Si alloys thus persists even after the material shows ferromagnetism with Curie temperature as high as $77^O$K and above. The persistence of upturn effect was also observed for Cr-Fe-Al alloys upto $(Cr_{70}Fe_{30})_{90}Al_{10}$ alloy(and possibly slightly beyond this) which is known to be at the border line of non-ferromagnetic to ferro-magnetic states[34]. However, it is quite possible that with increasing Fe content the present series of Cr-Fe-Si alloys pass

through a more complex sequence of magnetic structures than given
by the comparatively simple sequence: anti-ferromagnetism (Cr-Si)→
super paramagnetic cluster formation → increase in the cluster
number density → long range ferromagnetic order (Cr:Fe < 80:20).
In the binary Cr-Fe alloys Ishikawa et al.[58] have indicated the
probable existence of a more complex magnetic structure than that
suggested by the simple sequence described above.

The prevalence of complex magnetic structures in the Cr-Fe
binary and the Cr-Fe based ternary alloys which make unambiguous
determination of $\gamma$ and $\beta$ difficult is still further illustrated by
the $(Cr_{90}Fe_{10})_{97}Si_3$ alloy. The C/T vs. $T^2$ plot of this alloy is
shown in Figure 10. There is a distinct droop in the curve below
$1.5^{\circ}K$, whereas at higher temperatures it is a straight line. The
analogous binary alloy $(Cr_{90}Fe_{10})$ has a simple straight line
C/T vs. $T^2$ relationship with a large slope.[21] Ishikawa et al.[58]
suggested that the magnetic structure of the alloy is quite com-
plex, and that there is a $T^3$ dependent contribution, other than
that originating from the lattice vibration, to the total specific
heat. If this is so, then, the apparent value of $\beta$ would be large.

The straight line portion of the C/T vs. $T^2$ plot of the
$(Cr_{90}Fe_{10})_{97}Si_3$ alloy has a small slope as against the large
slope in its binary counterpart. It is also interesting to note
that no such anomaly is found in the Cr-Fe-Al alloys. The distinct
droop in the C/T vs. $T^2$ plot similar to that in the present ternary
$(Cr_{90}Fe_{10})_{97}Si_3$ alloy was earlier reported for the binary $Fe_{65}Al_{35}$
alloy, and it was attributed to the existence of a complex magnetic

structure [31]. The present alloy with its high $\gamma$ and low $\beta$, both calculated from the straight line portion of the C/T vs. $T^2$ plot, as also the anomaly in the low temperature region suggests that complex magnetic interactions are active in it.

In the present series of (Cr-Fe-Si) alloys those with Fe content greater than 19.40 at% are ferromagnetic according to the simple test described earlier. Out of these ferromagnetic alloys those with 19.40 at% Fe, 24.25 at% Fe and 29.10 at% Fe belong to the group showing upturn anomaly in their C/T vs. $T^2$ plots. The remaining three alloys with 48.5 at% Fe, 72.75 at% Fe and 92.15 at% Fe are strong ferromagnets with their Curie temperatures above the ambient temperature, 25°C. The specific heat data for each of these latter alloys, as indicated earlier, fall on a straight line in a C/T vs. $T^2$ plot. Experimental work on the variation of magnetisation with temperature for Ni and Fe shows[59] that the magnetisation follows the $T^{3/2}$ law of spin wave theory. The existence of spin wave contribution in ferromagnetic Ni and Fe, though a small fraction of the total specific heat, has been reported by Dixon et al.[67] Assuming the presence of spin waves in the ferromagnets whilst also retaining the contributions from the other sources the molar specific heat may be written in the form,

$$C = A + \gamma T + \beta T^3 + \alpha T^{3/2} \tag{5.4}$$

for the alloys showing upturn effects, and

$$C = \gamma T + \beta T^3 + \alpha T^{3/2} \tag{5.5}$$

for the alloys with Fe content greater than 48.5 at% which apparently have normal straight line $C/T$ vs. $T^2$ plots.

The analysis of the data for the alloys with 19.40 at% Fe 24.25 at% Fe and 29.10 at% Fe, all of which show up turn anomaly in $C/T$ vs. $T^2$ plots, based on the equation (5.4) using the method of least squares are shown in Table 17. For each of the three alloys there is a large increase in A, a substantial decrease in $\gamma$ when the equation (5.4) is used as against the three parameter equation (4.3). The $\theta_D$ values for the alloys with 19.40 at% Fe and 24.25 at% Fe increased substantially making them comparable to those of their binary counterparts. However, for the alloy with 29.10 at% Fe the increase in $\theta_D$ is only marginal.

An attempt to fit the specific heat data for the alloys with Fe content greater than 48.5 at% to the equation (5.5) resulted in physically unacceptable solution as shown in Table 17, in the sense that $\alpha$ turned out to be a small negative value for each of the three alloys (with 48.5 at% Fe, 72.75 at% Fe and 92.15 at% Fe). The specific heat data for these three alloys, shown in Figures 12 and 13 show very little scatter. Considering the accuracy of the specific heat data for these alloys and also the results of Dixon et al.[67] our results seem to be somewhat strange. However, it is probable that the unrestricted solution of the specific heat equations in general donot allow correct evaluation of the different parameters involved in them. This has earlier been realised[34,37] for Cr-Fe-Al alloys where unrestricted solution of the three parameter equation (4.3) yielded

... temperature specific heat of $(Cr_x Fe_{1-x})_{97} Si_3$ alloys including the spin wave enhancement factor.

| Alloy Composition | Cr:Fe | $A \times 10^4$ (Cal.mol$^{-1}$ deg.$^{-1}$) | $\gamma(T) \times 10^4$ (Cal.mol$^{-1}$ deg.$^{-2}$) | $\beta(T^3) \times 10^4$ (Cal.mol$^{-1}$ deg.$^{-4}$) | $\alpha(T^{3/2}) \times 10^4$ (Cal.mol$^{-1}$ deg.$^{-5/2}$) | $\theta_D$ (°K) | RMS deviation of $C \times 10^4$ (Cal.mol$^{-1}$ deg.$^{-1}$) | Remarks |
|---|---|---|---|---|---|---|---|---|
| $Cr_{77.60}Fe_{19.40}Si_{3.00}$ | 80:20 | 7.389 | 38.59 | 0.2439 | - | 267 | 1.010 | Eqn.(4.3) |
| | | 11.864 | 31.15 | 0.1555 | 3.887 | 310 | 1.024 | Eqn.(5.4) |
| $Cr_{72.75}Fe_{24.25}Si_{3.00}$ | 75:25 | 10.745 | 23.67 | 0.2790 | - | 255 | 0.723 | Eqn.(4.3) |
| | | 16.019 | 14.18 | 0.1483 | 0.153 | 315 | 0.722 | Eqn.(5.4) |
| $Cr_{67.90}Fe_{29.10}Si_{3.00}$ | 70:30 | 12.55 | 16.25 | 0.3688 | - | 242 | 1.058 | Eqn.(4.3) |
| | | 16.51 | 9.10 | 0.2696 | 3.883 | 258 | 1.095 | Eqn.(5.4) |
| $Cr_{48.50}Fe_{48.50}Si_{3.00}$ | 50:50 | - | 13.74 | 0.1130 | - | 345 | 0.42 | Eqn.(1.1) |
| | | - | 15.81 | 0.2160 | -1.895 | 278 | 2.16 | Eqn.(5.5) |
| $Cr_{24.50}Fe_{72.50}Si_{3.00}$ | 25:75 | - | 10.19 | 0.0742 | - | 397 | 0.30 | Eqn.(1.1) |
| | | - | 11.32 | 0.1144 | -0.901 | 343 | 0.27 | Eqn.(5.5) |
| $Cr_{4.85}Fe_{92.15}Si_{3.00}$ | 5:95 | - | 10.39 | 0.0983 | - | 362 | 0.41 | Eqn.(1.1) |
| | | - | 11.49 | 0.1351 | -0.858 | 325 | 0.38 | Eqn.(5.5) |

negative values of $\beta$. It is quite likely that in the present case
a restricted solution of the equation (5.5), rather than the
unrestricted solution by the least squares method, using the
value of $\beta$ obtained by other techniques like the elastic constant
measurements would be helpful in evaluating the true value of $\alpha$
and hence the spin wave contribution to the specific heats.

The results of the electronic specific heat measurements
for the present series of ternary alloys containing Si are shown
inFigure 16 as a $\gamma$ vs. e/a plot. The results for the binary Cr-Fe
and the ternary Cr-Fe with 10 at% and 20 at% Al alloys are also
shown. In this figure the electronic specific heat coefficient $\gamma$
for the ternary alloys are plotted as a function of electron
concentrations corresponding to the composition in the transition
metals only, disregarding entirely the Al or Si content. It is
apparent that the curve for the Cr-Fe-Si alloys is somewhat
different from the binary Cr-Fe alloys and the ternary alloys
of Cr-Fe with 10 and 20 at% Al. For the Cr-Fe alloys with
10 at% Al there is practically no change in the $\gamma$ vs.e/a plot
from that of the binary Cr-Fe alloys. This has been interpreted
in terms of lack of interaction between the conduction electrons
of Al and the 3d band, indicating localisation of $3s^2 3p$ electrons
of Al. The nature of the curve for the 20 at% Al series, the
composition at which the magnetic moment per atom in the Fe-Al
alloys deviate from that given by simple dilution, is different.
In this case the curve for e/a > 6 shifts towards higher transi-
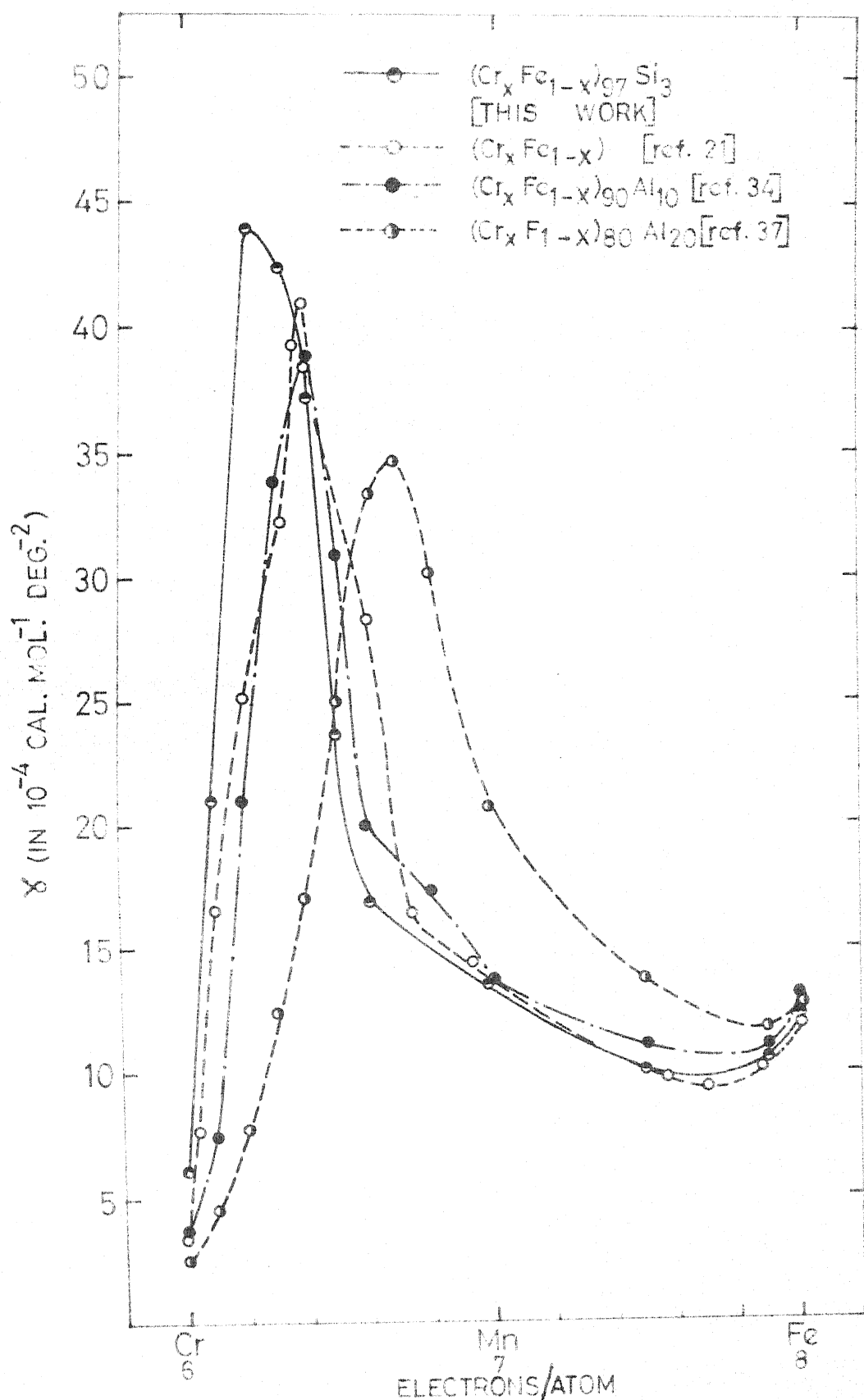tion metal electron concentration, which is equivalent to

Fig. 16 ELECTRONIC SPECIFIC HEAT COEFFICIENT OF $(Cr_x Fe_{1-x})_{97} Si_3$, $(Cr_x Fe_{1-x})$, $(Cr_x Fe_{1-x})_{90} Al_{10}$, $(Cr_x Fe_{1-x})_{80} Al_{20}$ ALLOYS

electron depletion from the 3d band. It has been noted[37] that the shift is not uniform. In the second sub-band the shift at $e/a = 8$ is greater than that at $e/a < 8$. In contrast, the curve for the Cr-Fe-Si alloys has shifted, compared to the Cr-Fe series of alloys, towards lower transition metal electron concentration. The general features of the second subband, with a prominent high peak, are retained. However, the peak height, position and also the peak breadth have increased. It is, however, possible that the anomolous $C/T$ vs. $T^2$ relation of the $(Cr_{90}Fe_{10})_{97}Si_3$ alloy prevented correct evaluation of $\gamma$, thereby showing an apparent increase in the breadth as well as the shift of the peak to $e/a = 6.2$. The data of the $(Cr_{95}Fe_5)_{97}Si_3$ and $(Cr_{85}Fe_{15})_{97}Si_3$ alloys, however, appear to be reliable because their specific heat data could be fitted well with the three term equation (4.3) and thus the shift of the $\gamma$ peak is real. In the particular representation employed in Figure 16, the results of the Cr-Fe-Si alloys would correspond to a filling up of the 3d band by the conduction electrons of Si. From the peak position of the binary Cr-Fe alloys at $e/a = 6.38$, and that of the Cr-Fe-Si alloys at $e/a = 6.2$, it appears that d band filling is to the extent of about 0.2 electrons at the high Cr side. Like the Cr-Fe-20 at% Al alloys, the shift of the $\gamma$ vs. $e/a$ curve for the Cr-Fe-Si alloys is not uniform throughout the whole $e/a$ range. It is larger in the high Cr range, $6.8 > e/a > 6$ where all the alloys exhibit anomolous $C/T$ vs. $T^2$ curves. In the high Fe

side of the alloy series, $e/a > 7$, the shift of the curve is
only marginal. The alloys in the latter composition range are
all distinctly ferromagnetic and they exhibit normal straight
line $C/T$ vs. $T^2$ curves. Magnetic data of Fe-Si alloys[60] show
that upto 10 at% Si the change in the moment per atom is due
only to simple dilution. Therefore, it is expected that the Si
solute, present to the extent of 3 at%, in Fe neither develops
any moment nor its conduction electrons have any appreciable
interaction with the 3d band of Fe. Such magnetic data, within
the purview of rigid band approximation, cannot explain the
nature of the shift which is marginal towards high Fe side
($e/a > 7$) and large in the high Cr side ($6 < e/a < 7$) of the
present Cr-Fe-Si series of alloys.

Theoretical investigations of Heine[61], and more recently
by Hodges et al.[62] indicate that in the first long period transi-
tion metal series the 3d band width of Cr is comparatively larger
than that of Fe. sd hybridisation is also larger in Cr than it
is in Fe. The 3d band being highly dense and narrow in Fe there
would be only feeble interaction between the 3d wave functions
and the 4s conduction electron. It has often been presumed[63]
that at least three of the four $3s^2 3p^2$ conduction electrons of each
Si solute atom in Fe remain localised near the solute, shielding
the excess charge. Therefore, the remaining conduction electron
per Si solute atom in Fe would mix with the 4s conduction ele-
ctron wave function of Fe producing only dilution effect in the
magnetic moment of Fe-Si system. This also explains the present

observation that Si addition has only marginal effect on the electronic specific heat of the alloys with high Fe concentrations, $e/a > 7$. The early transition element Cr has large sd or probably spd hybridisation[64] and its 3d band is less dense. Therefore, the nonlocalised members of the four $3s^2 3p^2$ electrons of Si are expected to mix with the 3d wave functions of Cr, thereby raising the Fermi level. This probably is a possible reason for the reasonably large shift of the peak in the $\gamma$ vs. $e/a$ plot at the high Cr region of the present Cr-Fe-Si alloys.

# CHAPTER VI

## CONCLUSIONS

1.    The electronic specific heat coefficients of the alloy $Cr_{97} Si_3$ is larger than that of pure Cr while the Debye temperature $\theta_D$ of the binary alloy is much smaller than that of the pure element.  A small amount of Si dissolved in Cr increases the electronic as well as the lattice contributions to the molar specific heat.

2.    The magnetic structure of the ternary $(Cr_x Fe_{1-x})_{97} Si_3$ alloys is quite complex.  This is illustrated clearly by the anomolous C/T vs. $T^2$ curve of the alloy $(Cr_{90} Fe_{10})_{97} Si_3$. The curve which is a straight line at higher temperatures, has a distinct downward droop below about $1.5^o$k.

3.    The peak in the $\gamma$ vs. e/a plot of the ternary $(Cr_x Fe_{1-x})_{97} Si_3$ alloy system, compared to that of the binary $(Cr_x Fe_{1-x})$ alloy  system is higher.  The peak in the present ternary system corresponds to the alloy $(Cr_{90} Fe_{10})_{97} Si_3$, for which $\gamma$ was calculated from the straight line portion of the curve.  It is quite possible that the anomolous C/T vs. $T^2$ relation for this alloy prevented correct evaluation of $\gamma$ , thereby showing an apparent increase in the peak height over that of the binary $(Cr_x Fe_{1-x})$ system.

4.    Compared to the binary $(Cr_x Fe_{1-x})$ alloy system the $\gamma$ vs. e/a curve of the ternary $(Cr_x Fe_{1-x})_{97} Si_3$ has shifted

towards lower transition metal electron concentration indicating
a possible interaction between the conduction electrons of Si
with the 3d band of the transition metals. From the peak position
of the binary $(Cr_xFe_{1-x})$ alloys at e/a = 6.38 and that
of the $(Cr_xFe_{1-x})_{97}$ $Si_3$ alloys at e/a = 6.2, it appears that
the d band filling by the conduction electrons of Si is to
the extent of about 0.18 to 0.2 electrons.

# BIBLIOGRAPHY

1.  Hume-Rothery, W.: J. Inst. Metals 35, 295, 307 (1926).

2.  For later summary, Hume-Rothery, W., and G.V.Raynor:In: Structure of Metals and Alloys. London: Institute of Metals 1962.

3.  Jones, H.:   Proc.Roy. Soc. A 144, 225 (1934), Proc.Roy. Soc. A 147, 396 (1934), Proc. Phys. Soc. 49, 250 (1937).

4.  For example, Nevitt, M.V.: In:  Electronic Structure and Alloy Chemistry of the Transition Elements, ed. by P.A. Beck. New York: J. Wiley 1963, p.101.

5.  Raynor, G.V.: J. Inst. Metals 70, 531 (1944).

6.  Laves, F., and H. Witte: Metallwirtschaft. 15, 840 (1936).

7.  Bardos, D.I., K.P. Gupta, and P.A. Beck: Tr. Met.Soc. AIME 221, 1087 (1961).

8.  Singh, B.N., and K.P. Gupta: Met. Trans. AIME 3, 1427 (1972).

9.  Wallace, W.E., and R.S. Craig: In: Phase Stability in Metals and Alloys, ed. by P.S. Rudman, J. Stringer and R.I. Jaffee, New York: Mc Graw Hill 1967, p. 255.

10.  Beck, P.A., and coworkers: Two representative papers, T. Met. Soc. AIME 236, 40 (1966), ibid 236, 64 (1966).

11.  Jones, H.: In: Metallic Solid Solutions, ed. by J.Friedel and A. Guinier. New York: W. Benjamin 1963, Lect. IX.

12.  Hume-Rothery, W., and J. Roaf: Phil. Mag. 6, 55 (1961).

13.  Blandin, A.P.: In: Alloying Behaviour and Effects in Concentrated Solid Solutions, ed. by T.B. Massalski. New York: Gordon and Breach 1965, p. 50.

14.  Blandin, A.P.: Phase Stability in Metals and Alloys, ed. by P.S. Rudman, J. Stringer and R.I. Jaffee. New York: Mc Graw Hill 1967, p. 115.

15.  Heine, V.: In: Physics of Metals, ed. by J.M. Ziman. London: Cambridge University Press 1969, Vol. 1, p.1.

16. Heine, V., and D. Weaire: In: Solid State Physics, ed. by H. Ehrenreich, F. Seitz and D. Turnbull. New York: Acad. Press 1970, Vol. 24, p. 250.

17. Sieb, D.H., and W.E. Spicer: Phys. Rev. Letters 22, 774 (1969).

18. Sieb, D.H., and W.E. Spicer: Phys. Rev. B1, 937 (1970).

19. Wenger, A., G. Bürri, and S. Steinemann: Solid State Comm. 9, 1125 (1971).

20. Heininger, F., E. Bucher, and J. Muller: Phys. Kond. Mat. 5, 243 (1966).

21. Cheng, C.H., C.T. Wei, and P.A. Beck: Phys. Rev. 120, 426 (1960).

22. Gupta, K.P., C.H.Cheng, and P.A. Beck: In: Metallic Solid Solutions, ed. by J. Friedel and A.Guinier. New York: W. Benjamin, 1963, Lect. XIV.

23. Nemnonov, S.A.: Phys. of Metals and Metallography (English) 19 (no. 4), 66 (1965).

24. Beck, P.A.: J. of Research. N.B.S. 74A, 449 (1970).

25. Clune, L.C., and B.A. Green, Jr.: Phys. Rev. B1, 1459 (1970).

26. Grimvall, G.: Phys. Kond. Mat. 11, 279 (1971), ibid 14, 101 (1972).

27. Mizutani, U., S. Noguchi, and T.B.Massalski: Phys. Rev. B5, 2057, (1972).

28. Knapp, G.S., and R.W. Jones: Phys. Rev. B6, 1761 (1972).

29. McMillan, W.L.: Phys. Rev. 167, 331 (1968).

30. Beck, P.A.: Proc. Int. Conf. on Magnetism, Nottingham, Inst. Phys. and Phys. Soc. London (1964), p. 178.

31. Cheng, C.H., K.P. Gupta, C.T.Wei, and P.A. Beck: J.Phys. Chem. Solids 25, 759 (1964).

32. Gupta, K.P., C.H. Cheng, and P.A. Beck: J.Phys. Chem. Solids 25, 1147 (1964).

33. Arrott, A., and H. Sato: Phys. Rev. 114, 1420 (1959).

34. Pessall, N., K.P. Gupta, C.H. Cheng, and P.A. Beck: J. Phys. Chem. Solids, 25, 993 (1964).

35.  Lousama, O.V., C.H. Cheng, and P.A. Beck: Phys. Rev. 128, 2153 (1962).

36.  Srinivasan, T.M., H.Claus, R.Viswanathan, P.A.Beck and D.I. Bardos: In: Phase Stability in Metals and Alloys, ed. by P.S. Rudman, J. Stringer and R.I.Jaffee. New York: Mc Graw Hill 1967, p. 151.

37.  Srinivasan, T.M., and H. Claus: J. Phys. Chem. Solids 28, 711 (1967).

38.  Chakravarty, D.J., and P.A. Beck: J. Phys. Chem. Solids 32, 1609 (1971).

39.  Kiessling, R.: Met. Rev. 2, 77 (1957).

40.  Dempsey, E.: Phil. Mag. 8, 285 (1963).

41.  Nicholson, M.E.: T.Met. Soc. AIME 209, 1 (1957).

42.  Juretschke, H.J., and R. Steinitz. J. Phys. Chem. Solids 4, 118 (1958).

43.  Hanson, D., M. Mahnig, and L.E. Totch: Z. Naturforsch. 26, 738 (1971).

44.  Keesom, P.A., and N. Pearlman: In: Encyclopedia of Physics, ed. by ~S.Flugge.Vol. 14, 297 (1956).

45.  Cheng, C.H.: Thesis, Univ. of Illinois 1959.

46.  Massalski, T.B., G.A. Sargent, and L.L. Isaacs: In: Phase Stability in Metals and Alloys, ed. by P.S. Rudman, J. Stringer and R.I. Jaffee. New York: Mc Graw Hill 1967, p. 291.

47.  Hahn, A., and E.P. Wohlfarth: Helv. Phys. Acta 41, 857 (1968).

48.  Nevitt, M.V., and A.T. Aldred: J. Appl. Phys. 34, 463 (1963).

49.  Rajan, N.S., R.M. Waterstat, and P.A. Beck: J. Appl. Phys. 31, 731 (1960).

50.  Koehler, W.C., R.M. Moon, A.L. Trego, and A.R.Mackintosh: Phys. Rev. 151, 405 (1966).

51.  Herbert, I.R., P.E. Clark, and G.V.R. Wilson: J. Phys. Chem. Solids 33, 979 (1972).

52. Doniach, S., and S. Engelsberg: Phys. Rev. Letters 17, 750 (1966).

53. Brinkman, W.F., and S. Engelsberg: Phys. Rev. 169, 417 (1968).

54. Benneman, K.H.: Phys. Rev. 167, 564 (1968).

55. Schröder, K.: J. Appl. Phys. 32, 830 (1961).

56. Livingston, J.D., and C.P. Bean: J.Appl.Phys. 32, 1964 (1961).

57. Bucher, E., W.F. Brinkman, J.P. Maita, and H.J. William: Phys. Rev. Letters 18, 1125 (1967).

58. Ishikawa, Y., R. Tournier, and J. Fillipi: J.Phys. Chem. Solids 26, 1727 (1965).

59. Argyle, B.E., S.W. Charap, and E.W. Pugh: Phys. Rev. 132, 2051 (1963).

60. Parsons, D., W. Sucksmith, and J.E. Thomson: Phil. Mag. 3, 1174 (1956).

61. Heine, V.: Phys. Rev. 153, 673 (1967).

62. Hodges, L., R.E. Watson, and H. Ehrenreich: Phys. Rev. B5, 3953 (1972).

63. Stearns, M.B.: Phys. Rev. B6, 3326 (1972).

64. Goff, J.F.: Phys. Rev. B4, 1121, (1971).

65. Mott, N.F.: Adv. Phys. 13, 325 (1964).

66. Srinivasan, T.M., and P.A. Beck: Ann. Acad. Sci. Fennicae A6, 163 (1966).

67. Dixon, M., F.E. Hoare, T.M. Holden, and D.E. Moody: Proc. Roy. Soc. A285, 561 (1965).

# APPENDIX A

## PROCEDURE FOR USING WOOD'S METAL SOLDER

Wood's metal, having the advantage of being a low melting solder, is used for making the demountable calorimeter can joint, as the joint can be made without damaging the nearby electrical lead wire connections made with 60:40 tin-lead solder. However, Wood's metal is a difficult solder material to handle in the sense that it has inferior wetting property necessitating the use of corrosive acid flux. For good leak proof joint the following scheme was evolved and was found to give satisfactory results.

### Initial Tinning:

Before the electrical lead wires were inserted the copper collar of the calorimeter can and the lip of the calorimeter top were cleaned with coarse and fine emery papers, washed in running water and dried. The dried surfaces were tinned with 60:40 tin-lead solder uniformly, wiping away the excess solder material with a clean cloth. The tinned surface cleaned of excess rosin flux, forms excellent base for Wood's metal. The tinned surfaces were then coated with Wood's metal using acid flux.

### Acid Flux for Wood's Metal:

For the best performance several acid fluxes were tried. 1:5 dilute $H_3 PO_4$ worked well except that it has certain disadvantages. This flux is extremely corrosive and gives irritatin

pungent vapour. Its other great disadvantage is that it often leaves extremely adhering sticky scum preventing proper wetting of the surfaces concerned with the solder material. The zinc chloride flux proved satisfactory. Commercial grade. Zn was dissolved in L.R. grade dilute (1:2) HCl acid by keeping for about 48 hours, till the reaction was complete. Sufficient amount of Zn was used such that some of it remained undissolved. The supernatant liquid, made acidic by addition of a few drops of concentrated HCl, was used for flux.

## Joining Procedure:

For actual joining, the tinned and subsequently Wood's metal coated surfaces were wetted with flux and assembled. The solder material was put around the joint with a clean and tinned (with Wood's metal) low wattage solder iron. When enough material collected. the solder iron was moved around the joint. In a short time the solder material all along the joint melted, which when left to cool by itself produced good vacuum tight joint.

Table 18: Control switch positions for low temperature specific heat measurements.

| Operations | Switches | | | | | | | | | | | | | K-3 | | |
|---|---|---|---|---|---|---|---|---|---|---|---|---|---|---|---|---|
| | $D_1$ | $D_2$ | $D_3$ | RS-1 | RS-2* | $T_1$ | $T_2$ | $T_3$ | $T_4$ | $T_5$ | $T_6$ | $T_{11}$ | Function Knob | Range | Aux.Pot. Selector |
| Pot.Standardization | N | N | Th | 1 | - | o | off | - | on | off | on | off | Std. | - | - |
| Bt.curr.stdn. | | | | | | | | | | | | | | | |
| i=n 0-1mA | H | N | Th | 1 | - | on | on | 0.1mA | off | off | on | off | Aux. | 0.16 | n |
| i=1-10mA | E | N | Th | 1 | - | on | on | 1-10 mA | off | off | on | off | Aux. | 1.6 | n |
| Ther.Curr.Stdn. | | | | | | | | | | | | | | | |
| i=1μA | Th | N | Th | 1 | - | on | off | - | off | off | on | on | Aux. | 0.16 | 1 |
| Heater EMF | | | | | | | | | | | | | | | |
| i = 0-1mA | N | H | Th | 1 | - | on | on | 0-1 mA | off | off | on | off | EMF | 0.16/1.6 | - |
| i = 1-10mA | N | H | Th | 1 | - | on | on | 1-10 mA | off | off | on | off | EMF | 1.6 | - |
| Ther. EMF | | | | | | | | | | | | | | | |
| i = 1μA | N | Th | Th | 1 | - | on | off | - | off | off | on | on | EMF | 0.016/0.16 | - |
| Recorder Calibration | N | Th | Th | 2 | - | on | off | - | off | on | off | off | EMF | 0.016 | - |
| Recording | N | Th | Th | 3 | - | on | on | as req. | off | on | off | on | EMF | 0.016/0.16 | - |

D = DPDT Switch;    T = Toggle Switch;    RS = Rotary Switch;    N = In Neutral Position

H = In Heater Circuit;    Th = In Thermometer Circuit;    n = As required

* Set according to the voltage of the battery in the thermometer circuit.

# APPENDIX C

## CALCULATION OF SPECIFIC HEAT FROM EXPERIMENTAL DATA

The specific heat at constant volume is defined as,

$$C_v = (dE/dT)_v \qquad \text{(C-1)}$$

where dE is the change in energy of the system and dT the corresponding change in temperature. For solids near the absolute zero temperature,

$$C = C_p = C_v = (dE/dT) \qquad \text{(C-2)}$$

In the present investigation the supply of energy to the system is in the form of electrical energy $= i^2 Rt$, where i = heating current in mA, R = heater coil resistance in ohms and t = duration of a heat pulse in seconds. Hence, the specific heat equation can be written as,

$$C = \frac{i^2 \cdot R \cdot t}{n \cdot J \cdot (T_2 - T_1)} \times 10^{-6} \text{ cal.mol.}^{-1} \text{ deg.}^{-1} \qquad \text{(C-3)}$$

where n = total number of moles of the specimen, J = electrical equivalent of heat and $T_2$ and $T_1$ are the final and initial temperatures, respectively. In the expression (C-3) a correction is necessary because of the presence of the heater-thermometer assembly, sandwitched between the two halves of the specimen. Corrections needed to take into account the change in the heater resistance between $4.2°K$ and $1.4°K$ and the heat dissipation through the leads connecting the heater coil to the Kovar

plug in the calorimeter cap have already been indicated in equation (4.2).

The total heat capacity for the specimen and heater-thermometer assembly can be written as,

$$nC = n_s C_s + n_{Cu} C_{Cu} \qquad (C-4)$$

where $n_s$ and $n_{Cu}$ are the numbers of moles of the specimen and of the heater-thermometer assembly including the tying wire taken into account as copper, respectively; $C_s$ and $C_{Cu}$ are the specific heats of the specimen and of the heater-thermometer assembly, respectively. Since the specific heat of copper was    in the form of $C_{Cu} = \gamma_{Cu} T + \beta_{Cu} T^3$, the equation (C-3) can be rewritten as,

$$\frac{C_s}{T} = \left[ \frac{i^2 \cdot R_H \cdot t \cdot 10^{-2}}{n_s \cdot J \cdot T(T_2 - T_1)} - \frac{n_{Cu}}{n_s} \gamma_{Cu} \times 10^4 - \frac{n_{Cu}}{n_s} \beta_{Cu} T^2 \times 10^4 \right]$$

$$\times 10^{-4} \text{ cal.mol.}^{-1} \text{deg.}^{-2} \qquad (C-5)$$

where $T = \frac{1}{2}(T_2 + T_1)$, and $R_H$ is the effective heater resistance as indicated in the equation (4.1).

A 41880

**Date Slip**

This book is to be returned on the
date last stamped.

ME-1973-D-KUM-LOW